scarring (4–7). Fibrocytes share markers of myeloid cells (for example, CD45 and CD34) and mesenchymal cells [for example, type I collagen (Col I) and fibronectin] (4–8). Additionally, fibrocytes express chemokine receptors (for example, CCR2, CCR5, CXCR4, and CCR7) that are involved in the recruitment of fibrocytes to sites of fibrosis (4–7,9). To date, the potential involvement of fibrocytes in peritoneal fibrosis has not been investigated.

The p38 mitogen-activated protein kinase (p38MAPK) mediates an important intracellular signal transduction pathway by which signals from environmental stimuli are transmitted to the nucleus. At least 3 distinct groups of MAPKs have been identified: extracellular signal-regulated kinase, c-Jun N-terminal kinase, and p38MAPK (10). Activation of p38MAPK is involved in apoptosis, stress responses, and inflammation (10). Recent studies have revealed that p38MAPK phosphorylation is essential for the production of various chemokines, including monocyte chemoattractant protein 1 (MCP-1, also known as CCL2), and for the signal transduction of chemokine receptors such as CCR2, which is a cognate receptor for CCL2 (11–16). In addition, p38MAPK has been demonstrated to contribute to the pathogenesis of fibrotic conditions (17–21).

Taken together, the foregoing findings prompted us to examine the involvement of p38MAPK signaling in fibrocyte function and the pathogenesis of peritoneal fibrosis. Using a well-known model of peritoneal fibrosis (22) induced in mice by intraperitoneal injection of chlorhexidine gluconate (CG), we evaluated the role of p38MAPK signaling with respect to fibrocyte function in the pathogenesis of peritoneal fibrosis and whether blockade of p38MAPK signaling may be a beneficial approach for the treatment of progressive peritoneal fibrosis.

METHODS

MURINE MODEL OF PERITONEAL FIBROSIS

Inbred male C57BL/6 mice (8 weeks, 20 – 25 g) obtained from Charles River Japan (Atsugi, Japan) were divided into 4 groups. Peritoneal fibrosis was induced in 3 groups of the mice by intraperitoneal injection of 0.1% CG dissolved in 15% ethanol/saline every other day, over a period of 21 days as previously described (22,23). A specific p38MAPK inhibitor, FR167653 [16 mg/kg (FR16) and 32 mg/kg (FR32) daily], was dissolved in drinking water and orally administered to 2 of the CG groups starting 2 days before CG injection (15,16,24). Mice in each group (controls, $n = 5$; CG-only group, $n = 9$; CG+FR groups, $n = 10$) were humanely killed 21 days after the start of CG injection. All procedures used in the animal experiments complied with the standards set out in the guidelines for the care and use of laboratory animals of Kanazawa University.

TISSUE PREPARATION

One portion of peritoneal tissue from each mouse was fixed in 10% buffered formalin (pH 7.2), embedded in paraffin, cut at 4 μm, stained with hematoxylin and eosin or Mallory–Azan and observed under a light microscope. The thickness of the submesothelial collagenous zone above the abdominal muscle layer in cross-sections of the abdominal wall was defined as the peritoneal thickness, as previously described (22). In each image, peritoneal thickness was measured at 10 different points. Peritoneal cross-sections were observed by 2 investigators and averaged to determine the reported peritoneal thickness. Measurements of peritoneal thickness were performed by image analysis using Mac SCOPE (version 6.02: Mitani Corporation, Fukui, Japan).

DETECTION OF FIBROCYTES IN PERITONEUM BY IMMUNOHISTOCHEMICAL STUDIES

Fibrocytes were identified in tissue samples by dual immunohistochemical techniques using specific antibodies against CD45 and Col I as previously described (5). For the present analysis, formalin-fixed, paraffin-embedded sections were prepared as previously described. Briefly, tissue sections were incubated with rat anti-mouse CD45 polyclonal antibodies (R&D Systems, Minneapolis, MN, USA) and rabbit anti-mouse Col I polyclonal antibodies (Chemicon International, Temecula, CA, USA). The CD45 was visualized by incubating sections with fluorescein isothiocyanate–conjugated donkey anti-rat immunoglobulin G antibodies (Jackson ImmunoResearch Laboratories, West Grove, PA, USA). The Col I was visualized using Cy3-conjugated donkey anti-rabbit immunoglobulin G antibodies (Jackson ImmunoResearch Laboratories).

Fibrocytes in peritoneum were counted in all fields of the submesothelial zone and expressed as the mean number ± standard error of the mean (SEM) per square millimeter. In addition, dual immunostaining for CCR2 and Col I was performed to characterize fibrocytes in the peritoneum. The tissue sections were incubated with goat anti-mouse CCR2 antibody (GeneTex, Irvine, CA, USA) and rabbit anti-mouse Col I polyclonal antibodies (Chemicon International). Fibrocytes positive for both CCR2 and Col I in peritoneum were counted in all fields of the submesothelial zone and expressed as the mean number ± SEM per square millimeter.

DETECTION OF PHOSPHORYLATED P38MAPK–POSITIVE CELLS

Immunohistochemistry for phosphorylated p38MAPK (p-p38MAPK) was performed to clarify the localization of cells positive for that marker. Formalin-fixed and paraffin-embedded sections were incubated with rabbit anti-mouse p-p38MAPK polyclonal antibodies (Cell Signaling Technology, Danvers, MA, USA). Mesothelial cells positive for p-p38MAPK were counted and expressed as a percentage of total mesothelial cells. In addition, immunostaining for CD45 and p-p38MAPK was performed to characterize the cells dually positive for those markers. Of the dual-positive cells, spindle-shaped cells that were positive for both CD45 and p-p38MAPK were regarded as fibrocytes positive for p-p38MAPK. Those cells were counted in all fields of the submesothelial zone and expressed as the mean number ± SEM per square millimeter.

DETECTION OF CCL2-POSITIVE CELLS

Immunohistochemistry for CCL2 was performed to clarify the localization of CCL2-positive cells. Formalin-fixed and paraffin-embedded sections were incubated with rat anti-mouse CCL2 polyclonal antibodies (Hycult Biotechnology, Uden, Netherlands).

ISOLATION OF HUMAN FIBROCYTES FROM PERIPHERAL BLOOD

Fibrocytes were harvested and cultured as previously reported (7). Briefly, centrifugation of venous blood drawn from healthy donors ($n = 3$) on a Ficoll–metrizoate density gradient [$d = 1.077$ g/mL (Lymphoprep: Nycomed, Oslo, Norway)] according to the manufacturer's protocol was used to isolate total peripheral blood mononuclear cells. After 2 days of culturing in tissue-culture flasks containing Dulbecco Modified Eagle Medium [DMEM (Gibco–BRL Life Technologies, Carlsbad, CA, USA] supplemented with 20% heat-inactivated fetal calf serum [FCS (Gibco–BRL Life Technologies)], 100 U/mL penicillin (Gibco–BRL Life Technologies), and 100 µg/mL streptomycin (Gibco–BRL Life Technologies), nonadherent cells were removed by gentle aspiration, and the media were replaced. After 10 – 12 days, adherent cells were lifted by incubation in ice-cold 0.05% EDTA in phosphate-buffered saline. The crude fibrocyte preparations then were depleted by immunomagnetic selection of contaminating T cells, B cells, and monocytes using pan-T, anti-CD2; pan-B, anti-CD19; and anti-CD14 monoclonal antibody–coated microbeads (Miltenyi Biotec, Bergisch Gladbach, Germany). Cell purity was verified by flow cytometry using both mouse anti-human CD45 monoclonal antibody [Becton Dickinson (PharMingen), Franklin Lakes, NJ, USA] and rabbit anti-human Col I polyclonal antibodies (Chemicon International).

CULTURE CONDITION OF FIBROCYTES

Purified fibrocytes were incubated with transforming growth factor β1 [TGFβ1 (R&D Systems)] in a time-dependent manner. Briefly, purified human fibrocytes (1×106/mL) were transferred to 12-well plates (Corning, Corning, NY, USA) containing DMEM supplemented with 0.5% heat-inactivated FCS (10 ng/mL) and were cultured at 37°C in a humidified atmosphere with 5% CO2 in the presence of TGFβ1 for 0 – 24 hours. In parallel experiments, fibrocytes were pretreated with FR32 and then exposed to the TGFβ1.

REAL-TIME REVERSE-TRANSCRIPTASE POLYMERASE CHAIN REACTION

To determine transcripts for the α1 chain of procollagen type I (Col Iα1) and CCL2 in the peritoneum, total RNA was extracted from whole peritoneum. Similarly, total RNA was extracted from cultured human fibrocytes and was analyzed for the detection of transcripts of Col Iα1. Quantitative real-time polymerase chain reaction was performed on the ABI Prism 7900HT Sequence Detection System (Applied Biosystems, Foster City, CA, USA) as previously described (5). Murine beta-glucuronidase and human glyceraldehyde-3-phosphate dehydrogenase were used as polymerase chain reaction controls.

STATISTICAL ANALYSIS

Means and SEMs were calculated for all parameters determined in this study. Statistical analyses used the Wilcoxon rank-sum test, the Kruskal–Wallis test, and analyses of variance. A p value less than 0.05 was accepted as statistically significant.

RESULTS

EFFECT OF P38MAPK ON PERITONEAL FIBROSIS

Morphology changes were assessed by hematoxylin and eosin or Mallory–Azan staining. In normal mice, the peritoneal tissue consisted of a peritoneal mesothelial monolayer and an exiguity of connective tissues under the mesothelial layer [Figure 1(A)]. At day 21, the peritoneal samples of wild-type mice injected with CG showed marked thickening of the submesothelial compact

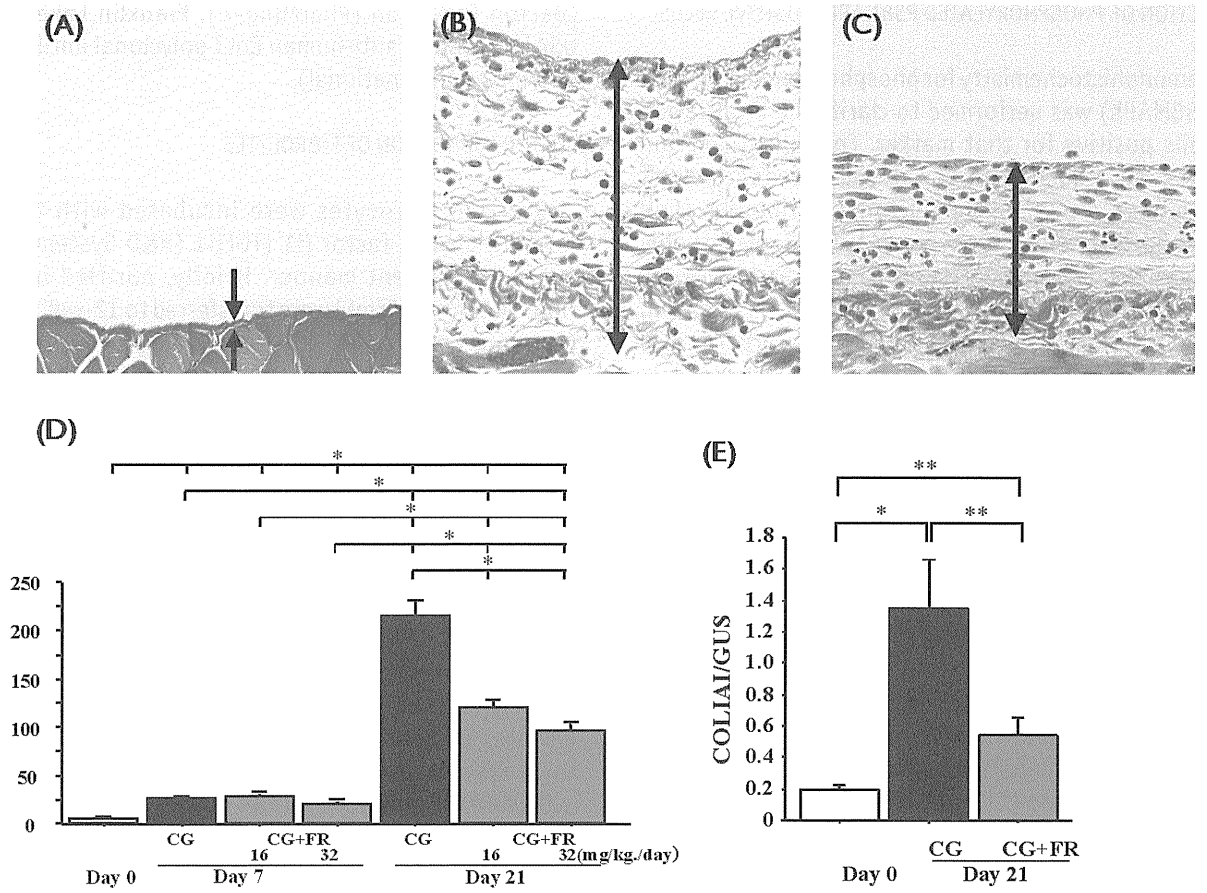

Figure 1 — Peritoneal thickness and type I collagen α1 (COLIAI) expression in the murine peritoneum. (A) Normal control at day 0 shows no evidence of peritoneal thickness (200× original magnification). (B) Peritoneal thickness at 21 days after the start of chlorhexidine gluconate (CG) injections ("CG mice") (200× original magnification). (C) Peritoneal thickness at day 21 in mice treated with FR167653 ("CG+FR mice") (200× original magnification). (D) Injection with CG caused the peritoneum to thicken in CG mice. By contrast, the peritoneum was less thick in CG+FR mice. (E) Upregulation of COLIAI messenger RNA expression was induced by CG injection and reduced with FR167653 treatment. Values are mean ± standard error of the mean. * $p < 0.01$. ** $p < 0.05$.

zone and the presence of numerous cells [Figure 1(B)]. By contrast, the thickness of the submesothelial zone and the number of infiltrating cells for peritonea from CG+FR mice were significantly less than those from CG mice [Figure 1(C)]. The mean peritoneal thickness, as determined by computer analysis, was less in CG+FR mice than in CG mice [Figure 1(D)]. The effect of FR32 was more marked than that of FR16. Therefore, in subsequent examinations, the data relating to the CG+FR32 group were used. The expression of Col Iα1 messenger RNA (mRNA) in peritoneum also was less with FR treatment [Figure 1(E)].

FIBROCYTES DUALLY POSITIVE FOR CD45/COL I INFILTRATE THE PERITONEUM

As originally reported, one of the unique characteristics of fibrocytes is their simultaneous expression of CD45 and Col I (4–9). To examine peritoneum for the presence of fibrocytes, immunostaining for both CD45 and Col I was performed. Such dually positive fibrocytes infiltrated the peritoneum after CG injection [Figure 2(A-C)]. The number of infiltrating fibrocytes increased with the progression of fibrosis after CG injection, but increased less in CG+FR mice (231.6 ± 27.9/mm^2) than in CG mice [616.0 ± 123.0/mm^2, Figure 2(D)].

CCR2-EXPRESSING FIBROCYTES AND PERITONEAL CCL2 EXPRESSION IN PERITONEUM

To better characterize fibrocytes infiltrating into peritoneum, dual immunostaining for CCR2 and Col I was performed. Numerous CCR2-positive fibrocytes were detected in peritoneum after CG injection [Figure 3(A-C)]. The number of CCR2-positive fibrocytes increased

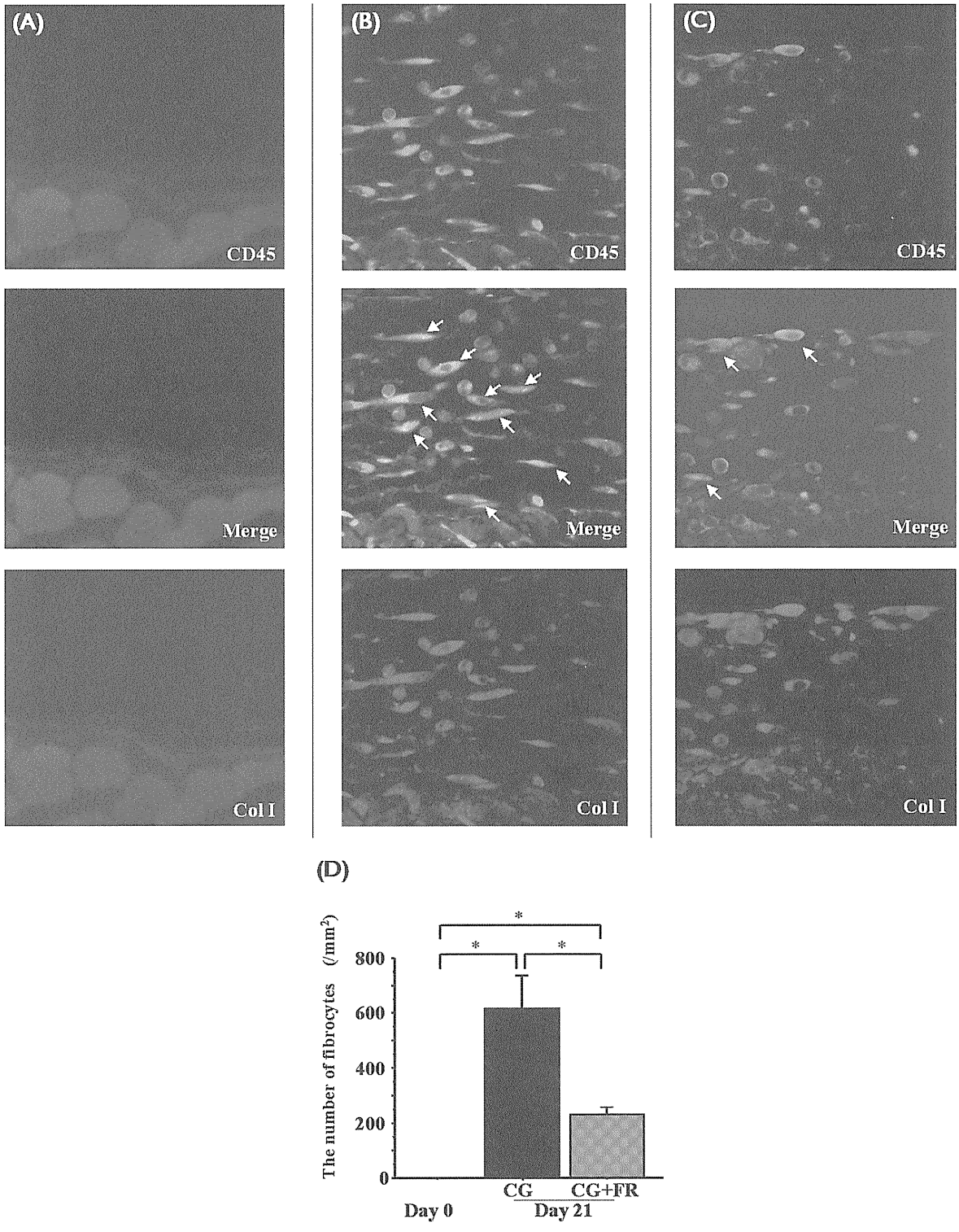

Figure 2 — Fibrocyte infiltration into peritoneum. Dual immunostaining for CD45 and type I collagen (Col I) was performed (green = CD45; yellow = dual-positive fibrocyte (arrows); red = Col I). Dual-positive fibrocytes infiltrated peritoneum after chlorhexidine gluconate (CG) injection. (A) Normal control at day 0 (200× original magnification). (B) Mice injected with CG (200× original magnification). (C) Mice injected with CG and treated with FR167653 (CG+FR) (200× original magnification). Arrows indicate cells that are dually positive for CD45 and Col I. (D) The number of infiltrating fibrocytes was lower in mice treated with FR167653. Values are mean ± standard error of the mean. * $p < 0.01$.

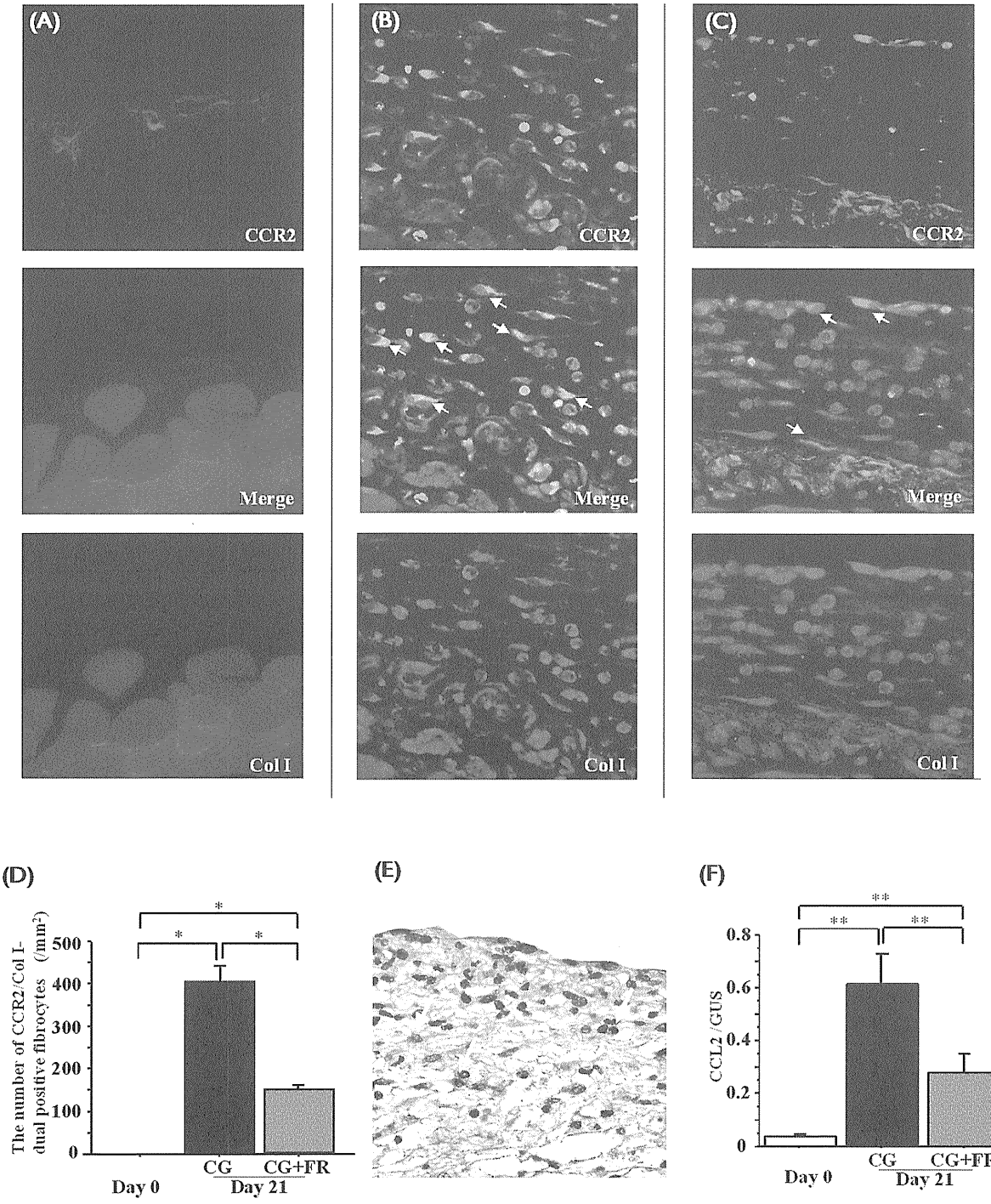

Figure 3 — Fibrocytes expressing CCR2, and CCL2 production, in peritoneum. Dual immunostaining for CCR2 and type I collagen (Col I) was performed (green = CCR2; yellow = CCR2-positive fibrocytes (arrows); red = Col I). Fibrocytes positive for CCR2 were detected in peritoneum after chlorhexidine gluconate (CG) injection. (A) Normal control at day 0. (B) Mice injected with CG. White arrows indicate cells positive for both CCR2 and Col I (200× original magnification). (C) Mice injected with CG and treated with FR167653 (CG+FR). White arrows indicate cells positive for both CCR2 and Col I (200× original magnification). (D) Fewer infiltrating CCR2-positive fibrocytes were observed in CG+FR mice. (E) Production of the CCL2 protein was induced by CG injection in peritoneal mesothelial cells as well as in interstitial cells. Yellow arrows indicate CCL2-positive cells (200× original magnification). (F) After CG injection, messenger RNA transcripts for CCL2 were upregulated in peritoneum; in CG+FR mice, levels of CCL2 were lower. Values are mean ± standard error of the mean. * $p < 0.01$. ** $p < 0.05$.

with the progression of fibrosis after CG injection, but increased less in CG+FR mice (150.9 ± 13.3/mm^2) than in CG mice [406.7 ± 39.8/mm^2, Figure 3(D)].

To elucidate the effect of p-p38MAPK signaling on peritoneal chemotactic molecules, expression of CCL2 was examined. Injection of CG induced the CCL2 protein in peritoneal mesothelial cells and in interstitial cells [Figure 3(E)]. In peritoneum, mRNA transcripts for CCL2 were upregulated after CG injection, and levels of CCL2 were lower in CG+FR mice [Figure 3(F)].

CELLS IN THE PERITONEUM POSITIVE FOR PHOSPHORYLATED P38MAPK

Immunohistochemical studies were performed to clarify the localization of p-p38MAPK–positive cells in the peritoneum. After CG injection, positivity for p-p38MAPK was detected in peritoneal mesothelial cells as well as in interstitial cells in thickened peritoneum [Figure 4(A)]. The percentage of p-p38MAPK–positive mesothelial cells was higher in CG mice than in CG+FR mice [Figure 4(B)]. In addition, the number of p-p38MAPK–positive interstitial cells in peritoneum was less in CG+FR mice than in CG mice [Figure 4(C)].

CELLS DUALLY POSITIVE FOR CD45 AND PHOSPHORYLATED P38MAPK IN PERITONEUM

To confirm the identity of peritoneal p-p38MAPK–positive cells, dual immunostaining for CD45 and p-p38MAPK was performed. A portion of these dually positive cells were spindle-shaped cells, suggesting the presence of p-p38MAPK–positive fibrocytes [Figure 5(A–C)]. The number of spindle-shaped cells dually positive for CD45 and p-p38MAPK in peritoneum was lower in CG+FR mice than in CG mice [Figure 5(D)].

PRODUCTION OF COL IA1 MRNA IN ISOLATED FIBROCYTES WAS REDUCED WITH FR167653 TREATMENT

The impact of p38MAPK signaling on Col Iα1 expression in isolated fibrocytes was examined *in vitro*. Circulating fibrocytes isolated from human peripheral blood (>97% pure population of cells co-expressing CD45 and Col I) were cultured in DMEM and 0.5% heat-inactivated FCS for 24 hours and were then stimulated with TGFβ1 (10 ng/mL) for 24 hours. Stimulation with TGFβ1 increased the expression of Col Iα1; pretreatment with FR167653 abrogated the TGFβ1-induced expression of Col Iα1 (Figure 6).

DISCUSSION

Using a murine model of peritoneal fibrosis, the present study provides evidence for infiltration by fibrocytes into peritoneum. The number of fibrocytes in peritoneum increased in accordance with the progression of peritoneal fibrosis. The infiltrating fibrocytes expressed the chemokine receptor CCR2, and an increase in p-p38MAPK was detected in peritoneal mesothelial cells and interstitial cells, including fibrocytes. The number of cells positive for p-p38MAPK and the level of peritoneal CCL2 expression were associated with the severity of fibrosis. Pharmacologic inhibition of p38MAPK signaling reduced the extent of fibrosis, the numbers of fibrocytes and of p-p38MAPK–positive cells, and the peritoneal expression of CCL2. Furthermore, inhibition of p38MAPK signaling attenuated the expression of Col Iα1 induced by TGFβ1

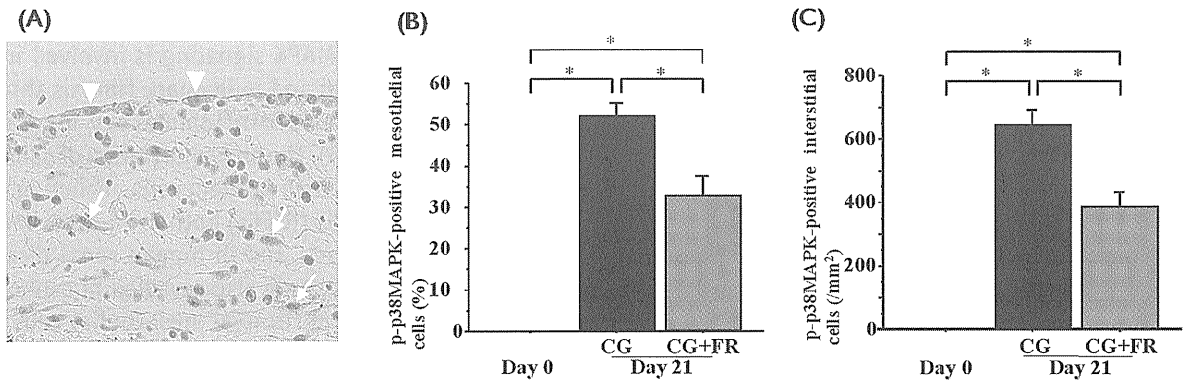

Figure 4 — The presence of cells positive for phosphorylated p38 mitogen-activated protein kinase (p-p38MAPK) in peritoneum. (A) Arrowheads indicate p-p38MAPK–positive mesothelial cells. Arrows indicate p-p38MAPK–positive spindle-shaped cells (200× original magnification). (B) The percentage of p-p38MAPK–positive mesothelial cells in peritoneum was lower in mice treated with FR167653 (CG+FR). (C) The number of p38MAPK-positive interstitial cells in peritoneum was significantly reduced in CG+FR mice. Values are mean ± standard error of the mean. * $p < 0.01$.

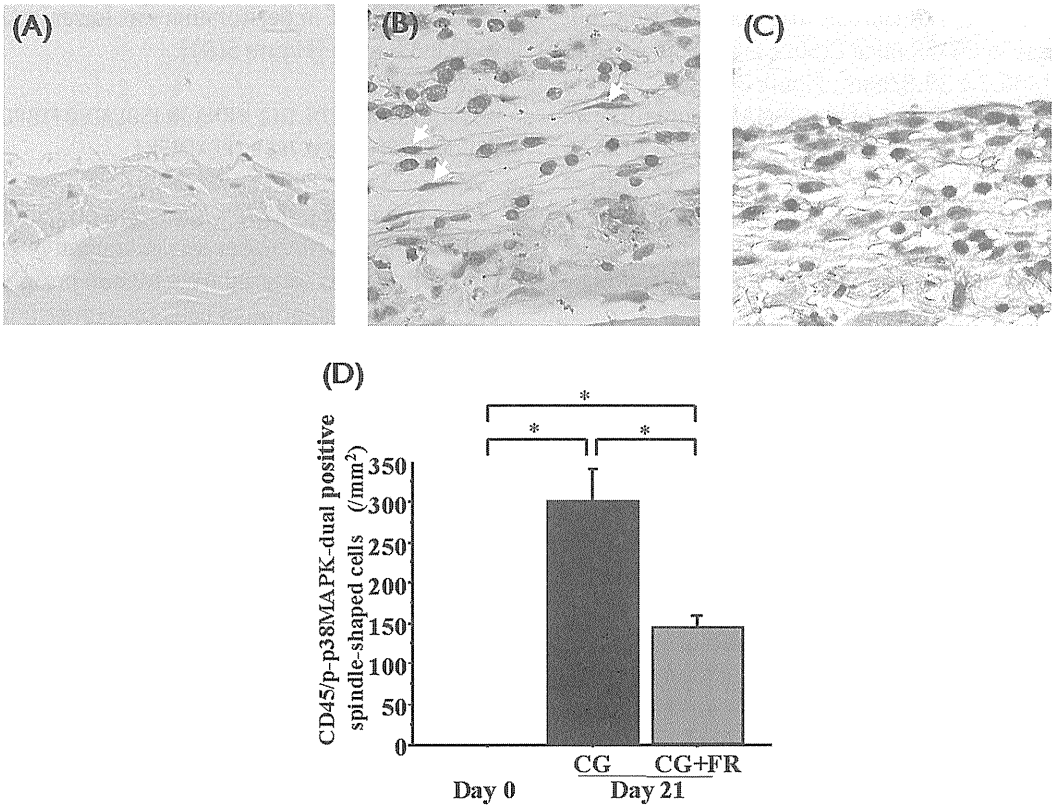

Figure 5 — Characterization of peritoneal cells positive for phosphorylated p38 mitogen-activated protein kinase (p-p38MAPK). Dual immunostaining for CD45 and p-p38MAPK was performed (brown = p-p38MAPK; red = CD45). Arrows indicate spindle-shaped cells positive for CD45 and p-p38MAPK. (A) Normal control at day 0 (200× original magnification). (B) Mice injected with CG (200× original magnification). (C) Mice injected with CG and treated with FR167653 (CG+FR) (200× original magnification). (D) The number of spindle-shaped cells positive for CD45 and p-p38MAPK was lower in CG+FR mice. Values are mean ± standard error of the mean. * $p < 0.01$. ** $p < 0.05$.

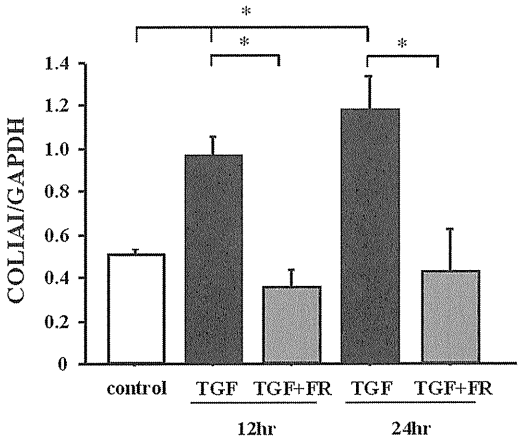

Figure 6 — The effect of p38 mitogen-activated protein kinase on production of procollagen type I α1 (COLIAI). Stimulation with transforming growth factor β1 (TGF) induced isolated fibrocytes to produce COLIAI messenger RNA, an effect that was reduced by treatment with FR167653 (FR). Values are mean ± standard error of the mean. * $p < 0.05$. GAPDH = glyceraldehyde 3-phosphate dehydrogenase.

stimulation of cultured fibrocytes. These results suggest that the p38MAPK pathway contributes to the pathogenesis of peritoneal fibrosis through activation of and infiltration by fibrocytes.

Activation of p38MAPK signaling is involved in the pathogenesis of renal and pulmonary fibrosis through the upregulation of proinflammatory mediators (10,11,17,18,20,21,25). The phosphorylation of p38MAPK has been demonstrated in resident cells, including renal tubular epithelial cells (RTECs) both in an experimental model of renal fibrosis and in human renal diseases (20,21). The present study also revealed phosphorylation of p38MAPK in peritoneal mesothelial cells. Not only peritoneal mesothelial cells but also RTECs have been reported to be capable of producing chemokines via p38MAPK signaling cascades (26,27). The number of p-p38MAPK–positive cells and the level of CCL2 expression in mesothelial cells both increased concomitantly with progression of fibrosis, and treatment with FR167653 reduced those changes. Based on those findings, p38MAPK

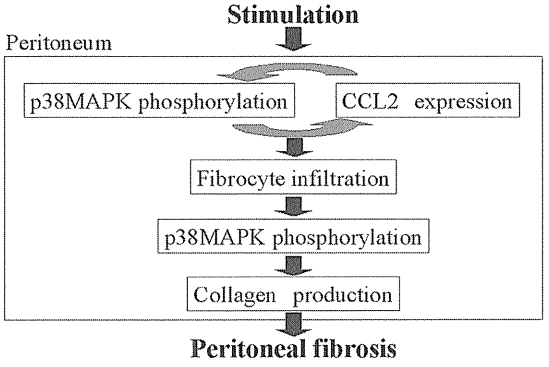

Figure 7 — Proposed schema for p38 mitogen-activated protein kinase (p38MAPK) signaling in the pathogenesis of peritoneal fibrosis: regulation of fibrocyte infiltration by production of CCL2 (a chemoattractant for fibrocytes), and production of collagen in fibrocytes.

may contribute to the production of CCL2 in peritoneal mesothelial cells, thereby promoting the pathogenesis of peritoneal fibrosis.

The infiltration of fibrocytes into diseased organs has been reported to be regulated by chemokine–chemokine receptor systems, including CCL2 and its receptor CCR2 (4–6,9,28). In addition, inhibition of the CCR2–CCL2 system has been shown to ameliorate the infiltration of fibrocytes and the severity of fibrosis in a murine pulmonary fibrosis model (9). In the present study, blockade of p38MAPK signaling reduced the number of CCR2-expressing fibrocytes in accord with levels of CCL2 expression and with the intensity of peritoneal fibrosis, suggesting that the CCR2–CCL2 system depends on p38MAPK. The potential roles of other chemokine systems, including CCR7–CCL21 and CXCR4–CXCL12, in the pathogenesis of peritoneal fibrosis remain to be determined.

Finally, we observed that the expression of Col Iα1 in cultured fibrocytes was enhanced by stimulation with TGFβ1 and that pretreatment with FR167653 abrogated the expression of Col Iα1. Thus, p38MAPK signaling may also contribute to the pathogenesis of peritoneal fibrosis by directly regulating the production of collagen in fibrocytes. Such a pathway has previously been suggested in studies of procollagen type I and fibronectin expression by scleroderma fibroblasts (29). Furthermore, CCR2-expressing fibrocytes have been shown, in a murine pulmonary fibrosis model, to express type I procollagen in response to stimulation with CCL2 (9).

CONCLUSIONS

Our results suggest that p38MAPK signaling is involved in the pathogenesis of peritoneal fibrosis through the regulation of fibrocyte infiltration and collagen production (Figure 7). Inhibition of the recruitment and activation of fibrocytes by p38MAPK signal transduction could provide a novel therapeutic approach for combating organ fibrosis.

ACKNOWLEDGMENTS

We are grateful to Professor Richard Bucala (Yale University) for careful review of the manuscript. This work was supported by a grant-in-aid from the Ministry of Education, Science, Sport and Culture of Japan (TW, NS), the Takeda Science Foundation (TW), and the Japan Baxter PD Fund (NS).

DISCLOSURES

The authors have no financial conflicts of interest to declare.

REFERENCES

1. Selgas R, Fernandez-Reyes MJ, Bosque E, Bajo MA, Borrego F, Jimenez C, *et al.* Functional longevity of the human peritoneum: how long is continuous peritoneal dialysis possible? Results of a prospective medium long-term study. *Am J Kidney Dis* 1994; 23:64–73.
2. Davies SJ, Bryan J, Phillips L, Russell GI. Longitudinal changes in peritoneal kinetics: the effects of peritoneal dialysis and peritonitis. *Nephrol Dial Transplant* 1996; 11:498–506.
3. Cnossen TT, Konings CJ, Kooman JP, Lindholm B. Peritoneal sclerosis—aetiology, diagnosis, treatment and prevention. *Nephrol Dial Transplant* 2006; 21(Suppl 2):ii38–41.
4. Phillips RJ, Burdick MD, Hong K, Lutz MA, Murray LA, Xue YY, *et al.* Circulating fibrocytes traffic to the lungs in response to CXCL12 and mediate fibrosis. *J Clin Invest* 2004; 114:438–46.
5. Sakai N, Wada T, Yokoyama H, Lipp M, Ueha S, Matsushima K, *et al.* Secondary lymphoid tissue chemokine (SLC/CCL21)/CCR7 signaling regulates fibrocytes in renal fibrosis. *Proc Natl Acad Sci U S A* 2006; 103:14098–103.
6. Abe R, Donnelly SC, Peng T, Bucala R, Metz CN. Peripheral blood fibrocytes: differentiation pathway and migration to wound sites. *J Immunol* 2001; 166:7556–62.
7. Sakai N, Wada T, Matsushima K, Bucala R, Iwai M, Horiuchi M, *et al.* The renin–angiotensin system contributes to renal fibrosis through regulation of fibrocytes. *J Hypertens* 2008; 26:780–90.
8. Bucala R, Spiegel LA, Chesney J, Hogan M, Cerami A. Circulating fibrocytes define a new leukocyte subpopulation that mediates tissue repair. *Mol Med* 1994; 1:71–81.
9. Moore BB, Kolodsick JE, Thannickal VJ, Cooke K, Moore TA, Hogaboam C, *et al.* CCR2-mediated recruitment of

fibrocytes to the alveolar space after fibrotic injury. *Am J Pathol* 2005; 166:675–84.
10. Wang XS, Diener K, Manthey CL, Wang S, Rosenzweig B, Bray J, *et al.* Molecular cloning and characterization of a novel p38 mitogen-activated protein kinase. *J Biol Chem* 1997; 272:23668–74.
11. Sakai N, Wada T, Furuichi K, Iwata Y, Yoshimoto K, Kitagawa K, *et al.* p38 MAPK phosphorylation and NF-kappa B activation in human crescentic glomerulonephritis. *Nephrol Dial Transplant* 2002; 17:998–1004.
12. Rovin BH, Wilmer WA, Danne M, Dickerson JA, Dixon CL, Lu L. The mitogen-activated protein kinase p38 is necessary for interleukin 1β-induced monocyte chemoattractant protein 1 expression by human mesangial cells. *Cytokine* 1999; 11:118–26.
13. Goebeler M, Kilian K, Gillitzer R, Kunz M, Yoshimura T, Bröcker EB, *et al.* The MKK6/p38 stress kinase cascade is critical for tumor necrosis factor-α–induced expression of monocyte chemo chemoattractant protein-1 in endothelial cells. *Blood* 1999; 93:857–65.
14. Furuichi K, Wada T, Iwata Y, Sakai N, Yoshimoto K, Kobayashi Ki K, *et al.* Administration of FR167653, a new anti-inflammatory compound, prevents renal ischemia/reperfusion injury in mice. *Nephrol Dial Transplant* 2002; 17:399–407.
15. Iwata Y, Wada T, Furuichi K, Sakai N, Matsushima K, Yokoyama H, *et al.* p38 Mitogen-activated protein kinase contributes to autoimmune renal injury in MRL–Fas lpr mice. *J Am Soc Nephrol* 2003; 14:57–67.
16. Wada T, Furuichi K, Sakai N, Iwata Y, Yoshimoto K, Shimizu M, *et al.* A new anti-inflammatory compound, FR167653, ameliorates crescentic glomerulonephritis in Wistar–Kyoto rats. *J Am Soc Nephrol* 2000; 11:1534–41.
17. Wada T, Furuichi K, Sakai N, Hisada Y, Kobayashi K, Mukaida N, *et al.* Involvement of p38 mitogen-activated protein kinase followed by chemokine expression in crescentic glomerulonephritis. *Am J Kidney Dis* 2001; 38:1169–77.
18. Wada T, Azuma H, Furuichi K, Sakai N, Kitagawa K, Iwata Y, *et al.* Reduction in chronic allograft nephropathy by inhibition of p38 mitogen-activated protein kinase. *Am J Nephrol* 2006; 26:319–25.
19. Sato M, Shegogue D, Gore EA, Smith EA, McDermott PJ, Trojanowska M. Role of p38 MAPK in transforming growth factor beta stimulation of collagen production by scleroderma and healthy dermal fibroblasts. *J Invest Dermatol* 2002; 118:704–11.
20. Stambe C, Atkins RC, Tesch GH, Masaki T, Schreiner GF, Nikolic–Paterson DJ. The role of p38alpha mitogen-activated protein kinase activation in renal fibrosis. *J Am Soc Nephrol* 2004; 15:370–9.
21. Sakai N, Wada T, Furuichi K, Iwata Y, Yoshimoto K, Kitagawa K, *et al.* Involvement of extracellular signal-regulated kinase and p38 in human diabetic nephropathy. *Am J Kidney Dis* 2005; 45:54–65.
22. Tanabe K, Maeshima Y, Ichinose K, Kitayama H, Takazawa Y, Hirokoshi K, *et al.* Endostatin peptide, an inhibitor of angiogenesis, prevents the progression of peritoneal sclerosis in a mouse experimental model. *Kidney Int* 2007; 71:227–38.
23. Ishii Y, Sawada T, Shimizu A, Tojimbara T, Nakajima I, Fuchinoue S, *et al.* A experimental sclerosing encapsulating peritonitis model in mice. *Nephrol Dial Transplant* 2001; 16:1262–6.
24. Iwata Y, Furuichi K, Sakai N, Yamauchi H, Shinozaki Y, Zhou H, *et al.* Dendritic cells contribute to autoimmune kidney injury in MRL-Faslpr mice. *J Rheumatol* 2009; 36:306–14.
25. Matsuoka H, Arai T, Mori M, Goya S, Kida H, Morishita H, *et al.* A p38 MAPK inhibitor, FR-167653, ameliorates murine bleomycin-induced pulmonary fibrosis. *Am J Physiol Lung Cell Mol Physiol* 2002; 283:L103–12.
26. Matsuo H, Tamura M, Kabashima N, Serino R, Tokunaga M, Shibata T, *et al.* Prednisolone inhibits hyperosmolarity-induced expression of MCP-1 via NF-kappaB in peritoneal mesothelial cells. *Kidney Int* 2006; 69:736–46.
27. Ho AW, Wong CK, Lam CW. Tumor necrosis factor-alpha up-regulates the expression of CCL2 and adhesion molecules of human proximal tubular epithelial cells through MAPK signaling pathways. *Immunobiology* 2008; 213:533–44.
28. Wada T, Sakai N, Matsushima K, Kaneko S. Fibrocytes: a new insight into kidney fibrosis. *Kidney Int* 2007; 72:269–73.
29. Ihn H, Yamane K, Tamaki K. Increased phosphorylation and activation of mitogen-activated protein kinase p38 in scleroderma fibroblasts. *J Invest Dermatol* 2005; 125:247–55.

OPEN ACCESS Freely available online

PLoS one

Glycoprotein Hyposialylation Gives Rise to a Nephrotic-Like Syndrome That Is Prevented by Sialic Acid Administration in GNE V572L Point-Mutant Mice

Mitutoshi Ito[1], Kazushi Sugihara[1], Tomoya Asaka[2], Tadashi Toyama[4], Toru Yoshihara[1,3], Kengo Furuichi[4], Takashi Wada[4], Masahide Asano[1]*

1 Division of Transgenic Animal Science, Advanced Science Research Center, Kanazawa University, Kanazawa, Japan, **2** Nanao National Hospital, Nanao, Japan, **3** Research Center for Child Mental Development, Kanazawa University, Kanazawa, Japan, **4** Department of Laboratory Medicine, Kanazawa University Graduate School of Medical Science, Kanazawa, Japan

Abstract

Mutations in the key enzyme of sialic acid biosynthesis, UDP-*N*-acetylglucosamine 2-epimerase/*N*-acetyl-mannosamine kinase, result in distal myopathy with rimmed vacuoles (DMRV)/hereditary inclusion body myopathy (HIBM) in humans. Sialic acid is an acidic monosaccharide that modifies non-reducing terminal carbohydrate chains on glycoproteins and glycolipids, and it plays an important role in cellular adhesions and interactions. In this study, we generated mice with a V572L point mutation in the GNE kinase domain. Unexpectedly, these mutant mice had no apparent myopathies or motor dysfunctions. However, they had a short lifespan and exhibited renal impairment with massive albuminuria. Histological analysis showed enlarged glomeruli with mesangial matrix deposition, leading to glomerulosclerosis and abnormal podocyte foot process morphologies in the kidneys. Glycan analysis using several lectins revealed glomerular epithelial cell hyposialylation, particularly the hyposialylation of podocalyxin, which is one of important molecules for the glomerular filtration barrier. Administering Neu5Ac to the mutant mice from embryonic stages significantly suppressed the albuminuria and renal pathology, and partially recovered the glomerular glycoprotein sialylation. These findings suggest that the nephrotic-like syndrome observed in these mutant mice resulted from impaired glomerular filtration due to the hyposialylation of podocyte glycoproteins, including podocalyxin. Furthermore, it was possible to prevent the nephrotic-like disease in these mice by beginning Neu5Ac treatment during gestation.

Citation: Ito M, Sugihara K, Asaka T, Toyama T, Yoshihara T, et al. (2012) Glycoprotein Hyposialylation Gives Rise to a Nephrotic-Like Syndrome That Is Prevented by Sialic Acid Administration in GNE V572L Point-Mutant Mice. PLoS ONE 7(1): e29873. doi:10.1371/journal.pone.0029873

Editor: Tadayuki Akagi, Kanazawa University, Japan

Received November 10, 2011; **Accepted** December 5, 2011; **Published** January 13, 2012

Funding: This work was supported in part by Grants-in-Aid for Scientific Research (B) (grant No. 19300144 and 22300142) (to M.A.) from the Ministry of Education, Culture, Sports, Science and Technology of Japan (http://www.mext.go.jp/english/). The funders had no role in study design, data collection and analysis, decision to publish, or preparation of the manuscript. No additional external funding was received for this study.

Competing Interests: The authors have declared that no competing interests exist.

* E-mail: asano@kiea.m.kanazawa-u.ac.jp

Introduction

UDP-*N*-acetylglucosamine 2-epimerase/*N*-acetyl-mannosamine kinase is a dual-function enzyme that catalyzes the rate-limiting step in sialic acid biosynthesis (Figure 1A) [1]. Mice with a null mutation in the *GNE* gene are embryonic lethal, indicating that GNE is essential for early embryonic development [2]. Human *GNE* mutations result in an adult-onset, progressive, autosomal recessive muscular disorder, distal myopathy with rimmed vacuoles (DMRV)/hereditary inclusion body myopathy (HIBM) [3–5]. Among the various *GNE* mutations, one *GNE* founder mutation (V572L) has been reported in Japanese families affected by DMRV [3].

Sialic acid is an acidic monosaccharide known to modify non-reducing terminal carbohydrates on glycoproteins and glycolipids, where it functions in cellular adhesions and interactions in the nervous and immune systems [6–8]. In renal functions, sialic acid residues are important in glomerular filtration, and their deficiency is implicated in proteinuria [9–13]. It has been reported that glomerular podocyte and podocyte foot process morphologies are maintained by the anionic charge of sialic acid residues on podocyte glycoproteins and glycolipids [12,14], and that a barrier to protein permeability is controlled by functional endothelial glycocalyx in glomeruli [15,16]. The glomerular filtration barrier, which consists of podocytes, the glomerular basement membrane (GBM), and fenestrated endothelial cells, prevents the leakage of albumin and other proteins from the blood stream by size- and charge-dependent filtration [15–17]. A lack of sialic acid residues on renal glycoproteins and glycolipids neutralizes their negative charge, disrupting the podocyte structure and resulting in massive proteinuria and podocytopathy [9,13,18,19]. For instance, it was previously shown that loss of podocyte foot processes was induced by the injection of puromycin aminonucleoside to neutralize the glomerular negative charge in normal rats [13,19]. However, it is still not clear whether the development of proteinuria is caused by the defects of sialic acid residues on podocyte glycoproteins and glycolipids.

To develop an animal DMRV model and clarify the role of sialic acid residues in the development of DMRV or other diseases, we generated mice with a kinase-domain point mutation (V572L) in GNE. Surprisingly, there were no apparent myopathic features or motor dysfunctions in the GNE V572L point-mutant homo-

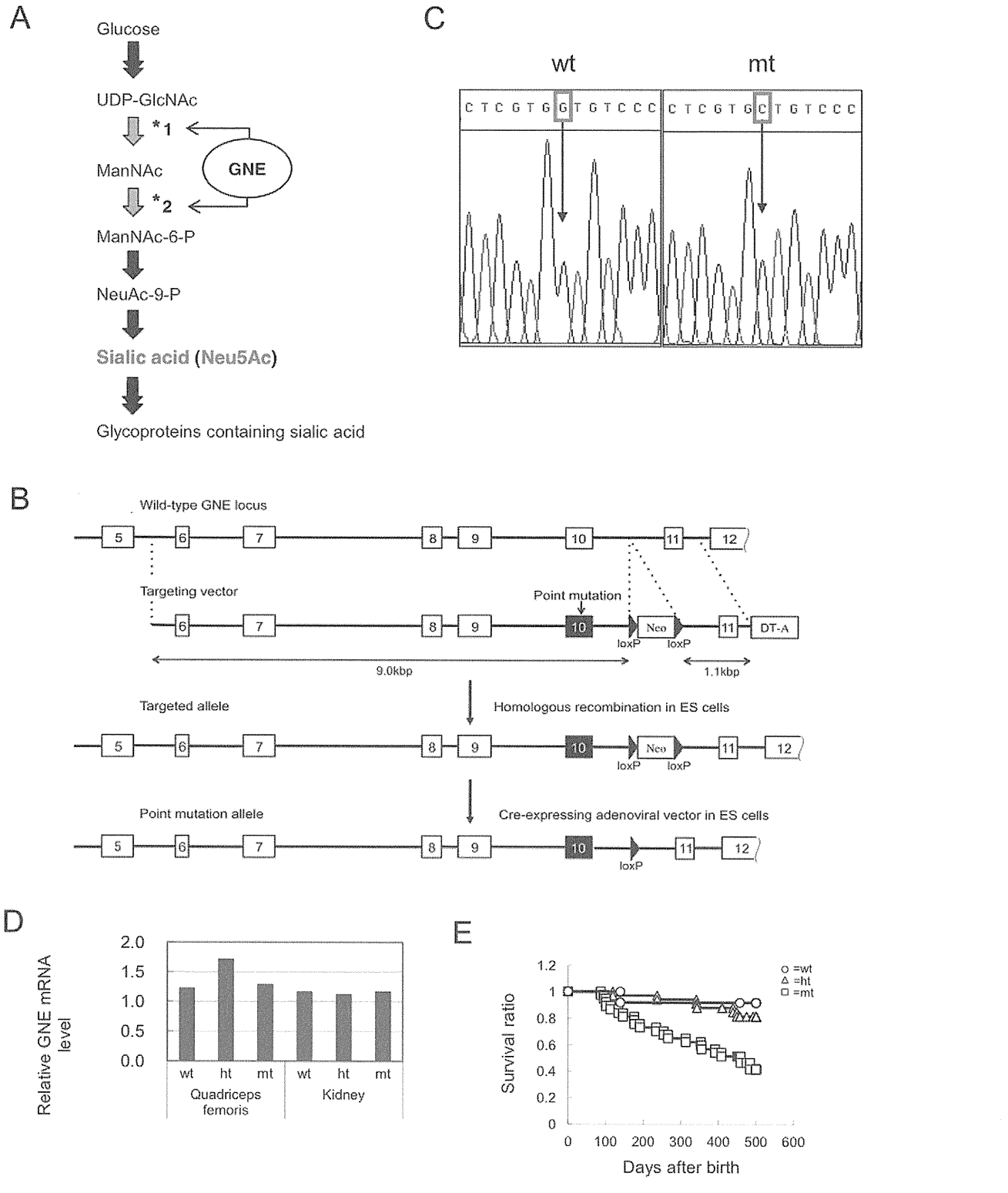

Figure 1. The sialic acid biosynthesis pathway and the generation of GNE V572L point-mutant mice. (**A**) The sialic acid biosynthesis pathway. GNE has dual-function enzymatic activity, UDP-*N*-acetylglucosamine-2-epimerase (*1) and *N*-acetylmannosamine kinase (*2), in the cytosol. (**B**) Targeting strategy to create a point mutation in exon 10 of the mouse *GNE* gene: to make the targeted allele, the wild-type GNE locus was replaced with a targeting vector, which contained a point mutation in exon 10, a neo cassette and a DT-A cassette, by homologous recombination. The neo cassette, flanked by two loxP sites, was deleted by a Cre-expressing adenoviral vector to make the point mutation allele. Neo, neomycin-resistance gene; DT-A, diphtheria toxin A fragment; triangles, loxP sites; open boxes with numbers, exons; closed boxes, exon 10 containing the point mutation. (**C**) A base exchange from G (wild-type; wt) to C (mutant; mt) at the 1714 site was confirmed by DNA sequencing. (**D**) Quantitative RT-PCR analysis of the *GNE* mRNA level normalized to the *GAPDH* mRNA level in the quadriceps femoris and kidney of the mutant (mt), heterozygous (ht), and wild-type (wt) mice. (**E**) Survival ratio of mt (squares, n = 37), ht (triangles, n = 33), and wt mice (circles, n = 12), analyzed by Kaplan Meier methods.
doi:10.1371/journal.pone.0029873.g001

zygous mice (mt-mice). However, the mt-mice had a short lifespan, massive proteinuria after birth, and abnormal kidney morphology.

Other than *GNE*-null mice, two *GNE* mutant mice have been reported previously. Transgenic mice expressing a human D176V point-mutant *GNE* gene in a mouse *GNE* knockout background develop myopathic disorders similar to DMRV [20], which are rescued by administering sialic acid metabolites [21]. However, no renal features have been described in these mice. On the other hand, another knock-in mouse carrying a GNE M712T point mutation cannot survive beyond 3 days due to severe glomerular hematuria, proteinuria, and podocytopathy [18]. Administering *N*-acetyl-mannosamine (ManNAc) partially suppresses these renal disorders and slightly prolongs their lifespan. However, these mutant mice do not display any myopathic features [18]. It is not clear why these two mice develop such different phenotypes.

Here, we present a third *GNE* mutant mouse, carrying a V572L mutation. This mouse shows renal but not myopathic features, much like the GNE M712T mutant [18]. However, our GNE V572L mutant mice have a much longer lifespan than the GNE M712T mutant. In this study, we examined the effect of hyposialylation caused by the GNE mutation on the renal disorders of the mt-mice, and attempted to suppress the renal disorders by administering 5-*N*-acetylneuraminic acid (Neu5Ac), a major sialic acid. We also evaluated the usefulness of the mt-mouse as an animal model of renal disease with proteinuria, such as congenital nephrotic syndrome (CNS) [17,22], and the potential of administering Neu5Ac as a therapeutic strategy to prevent renal disorders resulting from hyposialylation.

Materials and Methods

Generation of GNE V572L point-mutant mice

Mice containing a V572L point mutation in the *GNE* gene were generated using the ES-cell gene-targeting method. A targeting vector was constructed as follows (Figure 1B). The left arm (9.0 kb), containing exons 6 to 10, and the right arm (1.1 kb), containing exon 11, were amplified by PCR using a BAC clone (male CJ7/129Sv, Research Genetics, Huntsville, AL, USA) containing the mouse *GNE* gene as a template. DNA sequencing verified that there was no PCR error, at least in these exons. Primers used for amplifying exons 6, 7, 8, 9, 10 and 11 are listed in Table S1. A point mutation (G to C at the 1714 site) was created in exon 10 in the left arm using the Gene-editor in vitro Mutagenesis system (Promega Co, Madison, WI) according to the manufacturer's protocol, resulting in a change of Valine (GTG) to Leucine (CTG) at the amino acid 572 site in the GNE kinase domain. A *neo* cassette [23] flanked by two loxP sites was inserted between the left and right arms for positive selection, and a *DT-A* cassette [24] was ligated at the end of the right arm for negative selection. The resulting targeting vector is shown in Figure 1B.

The targeting vector was introduced into E14-1 ES cells (129/Ola strain) [25] by electroporation, and G418-resistant colonies were picked up as described previously [26]. We were only able to obtain one PCR-positive clone out of 670 colonies screened. Primers (GNE screening) used for PCR screening are listed in Table S1. DNA sequencing verified a point mutation in exon 10 of this clone using primers (GNE sequence) listed in Table S1. The homologous recombinant clone was infected with an adenoviral vector expressing the *Cre* gene [27] to delete the *neo* cassette in the genome, as shown in Figure 1B. Chimeric mice generated by the aggregation method [28] were mated with C57BL/6 mice to confirm germ-line transmission. The mt-mice on a mixed 129/Ola and C57BL/6 background, obtained by crossing heterozygous point-mutant mice (ht-mice), were used for experiments. Sex- and age-matched wild-type mice (wt-mice) and ht-mice were used as controls because the ht-mice did not show any renal disorder indistinguishable from wt-mice.

All mice were housed under specific pathogen-free conditions at the Institute for Experimental Animals of Kanazawa University. Animal experiments were conducted in strict accordance with the recommendations in the Fundamental Guidelines for Proper Conduct of Animal Experiments and Related Activities in Academic Research Institutions under the jurisdiction of the Ministry of Education, Culture, Sports, Science and Technology of Japan. The protocol was approved by the Committee on Animal Experimentation of Kanazawa University (Permit Number: AP-111959). All efforts were made to minimize suffering. All experiments were conducted according to the safety guidelines for gene manipulation experiments at Kanazawa University.

Genotyping by DNA sequencing and PCR

Mice were genotyped by the direct DNA sequencing of PCR products targeting the *GNE* gene exon 10, using genomic DNA taken from the mouse tail (Figure 1C, Table S1). Primers used for PCR are listed in Table S1. Alternatively, PCR genotyping was performed using allele-specific locked nucleic acid (LNA^{TM})-containing primers (Table S1) [29]. The PCR product of the wild-type allele (153 bp) of the *GNE* gene was amplified using primers 1 and 2, while the PCR product of the mutant allele (153 bp) was amplified using primers 1 and 3 (Figure S1A). PCR conditions were as follows: 98°C for 3 min, 20 cycles of 97°C for 20 s, 68.5°C for 30 s, and 72°C for 25 s, followed by 25 cycles of 96°C for 20 s, 52°C for 20 s, and 72°C for 15 s.

Rota-rod test

To investigate limb motor functions, we used the accelerating rota-rod paradigm [30]. Mice were tested in 3 trials per day for 3 consecutive days with a 300-s accelerating program (from 5 to 40 rpm), and the latency of the animal to fall from the rod was recorded.

Clinical chemistry test

Mice were placed individually in metabolic cages (Shinano Factory Co., Tokyo, Japan) for 24 hours with free access to food and water. Urine samples and heart serum samples were collected. Clinical chemistry tests of these samples, performed at the Nagahama Life Science Laboratory, measured the urine albumin, urine creatinine, serum albumin, and serum cystatin C. To analyze proteinuria in postnatal mice, urine samples (8 µl) were applied directly to SDS polyacrylamide gel electrophoresis (SDS-PAGE), and albumin was detected by Coomassie Brilliant Blue (CBB) staining.

Antibodies and lectins

The following primary antibodies and lectins were used for experiments: goat anti-mouse podocalyxin (R&D Systems, Inc., Minneapolis, MN), goat anti-mouse podoplanin (R&D Systems, Inc.), rabbit anti-mouse nephrin (Abcam, Tokyo, Japan), rabbit anti-mouse ezrin (Abcam), goat anti-mouse NHERF2 (Santa Cruz, Santa Cruz, CA), rabbit anti-mouse podocin (Santa Cruz), rabbit anti-mouse NEPH1 (Abcam), biotin-conjugated *Peanut agglutinin* (PNA) lectin (Seikagaku Biobusiness Co., Tokyo, Japan), biotin-conjugated *Ricinus communis Agglutinin* (RCA-I) lectin (Seikagaku Biobusiness Co.), *Dolichos biflorus agglutinin* (DBA) lectin (Vector Laboratories, Inc., Burlingame, CA), fluorescein isothiocyanate (FITC)-conjugated *Lotus tetragonolobus* (LTA) lectin (Vector Laboratories, Inc.), FITC-conjugated *Lycopersicon Esculentum* (LEL)

lectin (Vector Laboratories, Inc.), and Lectin Kit I, Fluorescein Labeled (Vector Laboratories, Inc, FLK-2100). PNA, RCA-I, DBA, LTA, and LEL recognized the following glycan structures: Galβ1-3GalNAc, Galβ1-4GlcAc, GalNAcα1-3GalNAc, L-Fucose, and GlcNAc oligomers, respectively.

The following secondary antibodies were used for experiments: Alexa Fluor 546-conjugated donkey anti-goat IgG (Life Technologies Japan, Ltd.,Tokyo, Japan), Alexa Fluor 488-conjugated goat anti-rabbit IgG (Molecular Probes, Eugene, OR), biotinylated goat anti-rabbit IgG (Vector Laboratories, Inc.), and biotinylated rabbit anti-goat IgG (Vector Laboratories, Inc.).

Histological analysis

Mouse kidneys were fixed in 10% neutral buffered formalin or 4% paraformaldehyde (PFA), respectively, in phosphate-buffered saline (PBS) (pH 7.4), then dehydrated and embedded in paraffin according to standard procedures. Tissue was sectioned (5 μm), deparaffinized, rehydrated, and stained with Periodic acid-Schiff (PAS) or Van-Gieson staining (a mixture of picric acid and acid fuchsin), each using standard methods. Fresh-frozen sections (10 μm) of mouse skeletal muscles were stained with modified Gomori trichrome staining method. For immunofluorescent staining, sections were deparaffinized and blocked with Super-Block blocking buffer (Pierce Biotechnology, Inc., Rockford, IL). They were incubated with anti-PC antibody (1/200 dilution) at 4°C overnight, incubated with Alexa Fluor 546-conjugated or Alexa Fluor 488-conjugated secondary antibodies (1/200 dilution) at room temperature (r.t.) for 2 hours, and mounted in ProLong Gold antifade reagent (Molecular Probes). Nuclei were stained with 4′, 6-diamidine-2-phenylindole (DAPI). Stained sections were observed under a fluorescence microscope (Olympus IX 71; Olympus, Corp., Tokyo, Japan) and confocal laser-scanning microscope (LMS510 META; Zeiss, Inc., Thornwood, NY).

For lectin staining, sections were deparaffinized and blocked with 0.1% Tween-20 in Tris-buffered saline (TBS) (pH 7.4), incubated with FITC-conjugated lectins (PNA, RCA-I, LTA, and DBA diluted 1/200) at r.t. for 2 hours, then mounted and observed.

Electron microscopy

Mouse kidneys were fixed with glutaraldehyde and osmium tetroxide, embedded in Epon 812 (Oken Shoji Co., Tokyo, Japan), and sliced into 0.1 μm sections. Sections were double-stained with uranyl acetate and lead citrate, and examined under an electron microscope (JEM-1210; JEOL Ltd., Tokyo, Japan) [31,32].

Western and lectin blotting

Frozen mouse kidneys were homogenized and dissolved in RIPA buffer, consisting of 50 mM Tris-HCl (pH 7.5), 150 mM NaCl, 1 mM EDTA, 0.5% NP-40, 0.5% sodium deoxycholate, 1.0% TritonX-100, and 0.1% SDS. Tissue lysates were centrifuged at 12,000× g at 4°C for 15 minutes to remove insoluble debris. The supernatants were mixed with Laemmli's sample buffer, consisting of 3% SDS, 5% glycerol, 1.67 mM Tris-HCl (pH 7.5), 0.05% bromophenol blue, and 10% 2-mercapto-ethanol, then boiled at 100°C for 3 minutes. The lysate protein concentration was measured using a BCA™ Protein Assay Kit (Pierce Biotechnology, Inc.) according to the manufacturer's protocol.

For Western blotting, proteins were separated by 12% or 8% SDS-PAGE using the Laemmli's buffer system, then transferred to PVDF membranes (Millipore Corp., Bedford, MA). After blocking with Block Ace (Yukijirushi Co, Ltd., Tokyo, Japan), the membranes were incubated overnight with primary antibodies (1/1000 or 1/500 dilution) at 4°C. After the membranes were treated with secondary antibody (1/2000 dilution) at r.t. for 30 minutes, the protein bands were detected with a Vectastain *Elite* ABC standard kit (Vector Laboratories, Inc.) and a Metal Enhanced DAB Substrate Kit (Thermo Scientific Inc., Rockford, IL) according to the manufacturers' protocols.

For lectin blotting, in brief, proteins were separated and transferred to PVDF membranes, as for Western blotting. After blocking with 0.05% Tween-20 in TBS, the membranes were incubated overnight with biotin-conjugated lectins at 4°C, and protein bands were detected as for Western blotting.

For neuraminidase treatment, 1 mU/μg neuraminidase from *Arthrobacter ureafaciens* (Nacalai Tesque, Inc., Kyoto, Japan) was added to the soluble proteins in the RIPA buffer and incubated at 37°C for 30 minutes. The desialylated proteins were mixed with Laemmli's sample buffer and boiled at 100°C for 3 minutes, and the lysates were used for Western blotting.

Immunoprecipitation

For immunoprecipitation, Protein G Sepharose 4 Fast Flow (GE Healthcare, Upsala, Sweden) was used according to the manufacturer's protocol. In brief, soluble kidney lysates prepared as the above Western blotting method were incubated with anti-PC antibody at 4°C for 1 hour with rotating, and then incubated with 50 μl of Protein G Sepharose at 4°C for 1 hour with rotating. Precipitated proteins were recovered by spin-down, washed, and then dissolved in Laemmli's sample buffer. The precipitated proteins were analyzed by Western and lectin blotting as described above.

Neu5Ac rescue experiments

Neu5Ac was administered as follows (Figure S2): briefly, pregnant ht-mice were left untreated or were treated with Neu5Ac (Nacalai Tesque, Inc.) (1 g/kg/day) in drinking water, from the time of mating through the nursing period. After weaning, pups were left untreated or were treated with Neu5Ac (0.2 g/kg/day) in the drinking water until 2 months of age; these Neu5Ac doses were selected based on other studies. [18,21]. The treated mice were sacrificed at 2 months old and analyzed by histological and biochemical methods.

Quantitative RT-PCR

Total RNA was extracted from mouse kidneys by the guanidine isothiocyanate method [33]. Complementary DNA (cDNA) was synthesized by a PrimeScript RT reagent kit (Takara Bio, Inc., Shiga, Japan), and real-time PCR amplification was performed using a Thermal Cycler Dice (Takara Bio, Inc.) with SYBR Premix Ex Taq II (Takara Bio, Inc.). The primer sequences are listed in Table S1. The PCR conditions were 94°C for 5 minutes, followed by 40 cycles of 94°C for 15 seconds, 60°C for 30 seconds, and a dissociation protocol. The mRNA copy numbers were calculated and normalized to the *GAPDH* mRNA levels.

Statistics

Statistical evaluation was performed using the Mann-Whitney U-test for clinical chemistry tests or Student's *t*-test for quantitative RT-PCR between the mt-mice and control mice. Two-way ANOVA was used for rescue experiments to confirm the effect of compound treatment and genotypes. A P-value<0.05 was considered statistically significant.

Results

Generation of GNE V572L point-mutant mice (mt-mice)

We generated mt-mice by the gene targeting method described in Materials and Methods (Figure 1B). A point mutation (G to C) at the 1714 site, resulting in a V572L mutation, was confirmed by DNA sequencing (Figure 1C). *GNE* mRNA levels in the

quadriceps femoris and kidney were comparable among the three genotypes—homozygous mutant (mt), heterozygous (ht), and wild-type—in spite of the point mutation (Figure 1D).

The mt-mice were born according to Mendelian inheritance and grew normally with a normal appearance. However, they began to die at around 100 days after birth, and about half of them died by 500 days (Figure 1E). Their kidneys appeared abnormal, being pale and irregularly shaped, but gross examination of various organs revealed no other abnormalities in these mice.

Severe albuminuria and high serum cystatin C levels in the mt-mice

We carried out urinary and serologic tests in the mice of various ages. The urinary albumin/creatinine ratio was markedly higher in the mt-mice than in control (wt and ht) mice at 3 and 6 months of age, while the serum albumin levels in the mt-mice were significantly lower than in control mice (Figure 2A, B), suggesting albumin leakage from the blood stream. Moreover, the serum cystatin C levels, which indicate the glomerular filtration rate (GFR) in humans, were also significantly higher in the mt-mice than in control mice (Figure 2C). At 10 days of age, albuminuria was already detectable by SDS-PAGE and CBB staining (Figure 2D). Differences in the urinary albumin/creatinine ratio and serum cystatin C level between mt and ht mice were not significant at 12–15 months old, probably because the severely affected mt-mice had already died, and only the less-affected mt-mice were still alive beyond 1 year.

Histological analysis of kidneys in the mt-mice

We examined PAS-stained renal sections of the mt-mice at 8 days, 3 months, 6 months and 12 months of age. At 8 days after birth, cast formation in the renal tubules consistent with albuminuria at the early postnatal stage was observed in the mt-mice. Glomeruli were enlarged in the mt-mice compared to

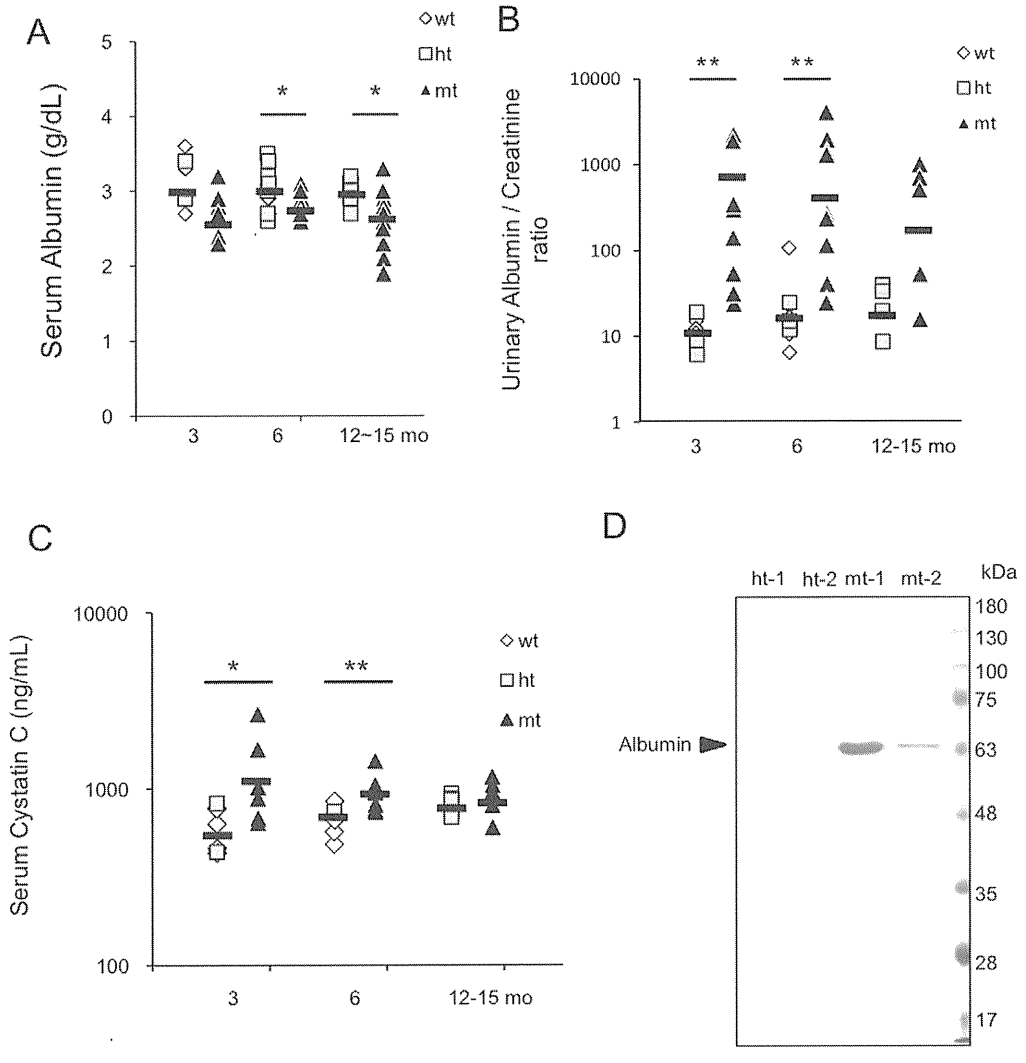

Figure 2. Clinical chemistry tests. (**A**) Serum albumin in wt (open diamonds), ht (gray squares), and mt (black triangles) mice at 3 months (n = 4 wt, 2 ht, 6 mt), 6 months (n = 9 wt, 3 ht, 9 mt), and 12–15 months (n = 1 wt, 11 ht, 12 mt). Data of the wt and ht mice are presented in the same column. (**B**) Urinary albumin/creatinine ratio in wt (open diamonds), ht (gray squares), and mt (black triangles) mice at 3 months (n = 8 wt, 3 ht, 9 mt), 6 months (n = 4 wt, 5 ht, 11 mt), and 12–15 months (n = 5 ht, 5 mt). (**C**) Serum cystatin C at 3 months (n = 4 wt, 2 ht, 6 mt), 6 months (n = 6 wt, 1 ht, 6 mt), and 12–15 months (n = 1 wt, 5 ht, 6 mt). (**D**) SDS-PAGE analysis of urinary proteins in ht and mt mice at 10 days after birth; 8 μl of urine was separated by SDS-PAGE and stained by CBB. Arrowhead: albumin band (60 kDa). Results are shown as means (bars) with individual data points (A, B, C). *$P<0.05$, **$P<0.01$ (Mann-Whitney U-test).
doi:10.1371/journal.pone.0029873.g002

ht-mice (Figure 3A, the first panel from the left). Glomerular lesions with mesangial matrix deposits, including glomerulosclerosis and enlarged Bowman's spaces as well as urinary tubule dilatation with cast, were observed at 3 months of age in the mt-mice (Figure 3A, the second panel from the left). At 6 and 12 months of age these glomerular lesions had progressed, and some mt-mice exhibited renal failure with severe glomerulosclerosis (Figure 3A, the third and forth panels from the left) and inflammatory cell infiltration in the interstitium (data not shown). In addition, Van-Gieson staining revealed interstitial fibrosis (Figure S3A). Consistent with these observations, tissue fibrosis markers such as *crlf*, *TGF-β*, and *CTGF* were significantly elevated in the kidneys of the mt-mice compared with those of ht-mice (Figure S3B). We further analyzed the ultrastructure of the podocyte foot processes and the filtration glomeruli barrier by electron microscopy; the podocyte foot processes of mt-mice at 4 months old were remarkably flattened and fused compared with the well-shaped foot processes of the wt-mice (Figure 3B).

Since glomerular lesions were observed shortly after birth, we examined whether nephron development was impaired. The size of the nephrogenic zone, where nephrons develop, and the number of nephrons in the cortex at 3 and 8 days after birth, respectively, were comparable between mt- and ht-mice, while the number of nephrons was significantly reduced in the 2-month-old mt-mice (Figure 4). These observations suggest that nephron development was normal in the mt-mice, but nephron maintenance was impaired.

Lectin staining of kidneys

To investigate the cell-surface glycan structures in the mt-mouse kidneys, we stained sections with several lectins, including PNA for Galβ1-3GalNAc, RCA-I for Galβ1-4GlcAc, LTA for L-Fucose, and DBA for GalNAcα1-3GalNAc (Figure 5A). In the mt-mouse kidneys, PNA-positive signals were aberrantly detected in glomeruli, and the RCA-I signals were more intense than in ht-mouse kidneys. High-magnification confocal microscopy revealed that PNA colocalized well with the epithelial cell marker podocalyxin (PC) in the mt-mouse glomeruli, while PNA was not observed in the ht-mouse glomeruli (Figure 5B). In contrast, PNA did not colocalize with the endothelial cell marker LEL in mt-mice; this indicates that PNA localized to glomeruli epithelial cells (Figure S4). PNA was observed in even immature glomeruli in 8-day-old mt-mice, but not in ht-mice (Figure 5C). These abnormal PNA and RCA-I signals suggested that glycoproteins and glycolipids in the mt-mouse kidneys, particularly in glomerular epithelial cells, were hyposialylated, since PNA and RCA-I recognize asialo glycans. On the other hand, the staining patterns of LTA and DBA, which recognize glycans with no relation to sialic acid, were comparable between the mt- and ht-mice, suggesting that the glycan structures recognized by LTA and DBA were not affected in the mt-mice.

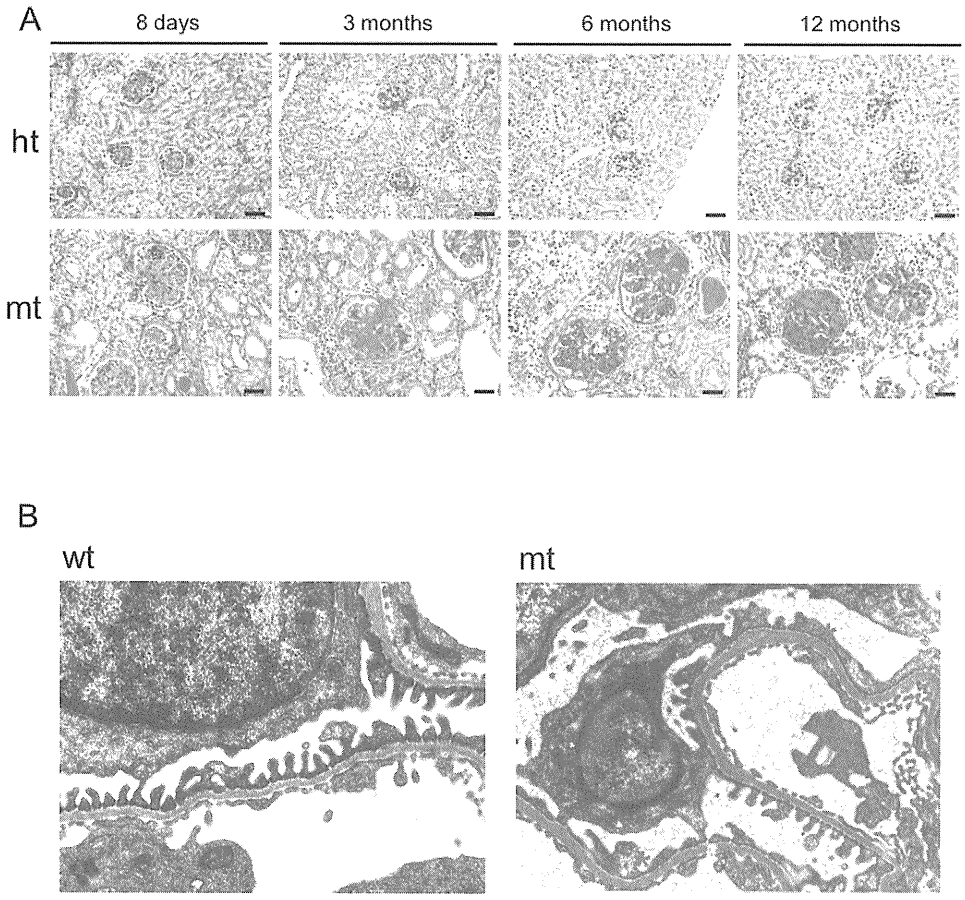

Figure 3. Histological kidney analysis. (A) PAS-stained kidney sections at 8 days, 3 months, 6 months and 12 months of age in ht (upper panels) and mt (lower panels) mice. Scale bars: 20 μm. (B) Electron microscopy of the glomeruli of wt (left panel) and mt mice (right panel) at 4 months old. Asterisks indicate flattened and fused podocyte foot processes.
doi:10.1371/journal.pone.0029873.g003

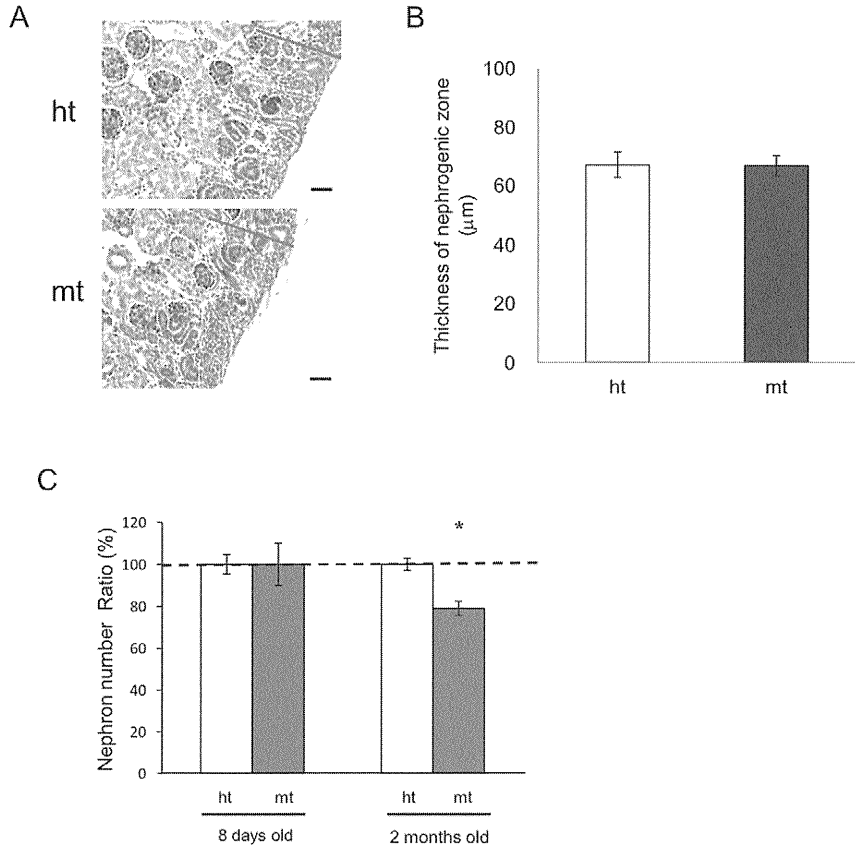

Figure 4. Nephrogenic zone formation and nephron numbers in kidneys. (A) PAS-stained kidney sections of ht (upper panel) and mt (lower panel) mice at 3 days after birth. Red bars indicate the nephrogenic zone. (B) Nephrogenic zone thickness compared between ht (open bars, n = 4) and mt (closed bars, n = 3) mice at 3 days after birth. (C) Relative nephron numbers compared between ht (open bars) and mt (closed bars) mice at 8 days (n = 10 ht, 9 mt) and 2 months (n = 6 ht, 6 mt) of age. Nephron number per mm^2 in the ht renal cortex at each age was designated as 100%. *$P<0.05$ (Mann-Whitney U-test).
doi:10.1371/journal.pone.0029873.g004

Hyposialylation of a major podocyte sialoprotein, podocalyxin (PC) in the mt-mice

Western blotting analysis of several renal proteins was performed using whole kidney lysates. There was no difference in the band intensity or mobility of NHERF2, ezrin, nephrin, podocin, podoplanin, or NEPH1 between the ht- and mt-mice (Figure S5). However, while 140–150 kDa bands of PC were detected in lysates from both the control and mt-mice, the lysates from mt-mice also produced higher molecular-weight 250-kDa smear bands by appearance (Figure 6A). Since sialoprotein hyposialylation gives rise to smear bands with higher molecular weights than expected, we treated the PC with neuraminidase (sialidase). The PC bands in neuraminidase-treated lysates from wt-mice shifted to about 250 kDa, much like the PC bands in untreated lysates from mt-mice (Figure 6B). We further investigated the PC glycan chains in the mt-mice by lectin blotting. The 250-kDa smear band could be detected in mt-mice lysates after immunoprecipitation with the anti-PC antibody (Figure 6C), and was detected only in these samples by the lectins RCA-I and PNA, which recognize asialo glycans (Figure 6D, E). These results collectively indicate that the PC in mt-mouse kidneys was highly hyposialylated.

Suppression of the renal disorders in mt-mice by Neu5Ac administration

If the hyposialylation of PC and other sialoproteins is a major cause of the renal disorders in mt-mice, administering Neu5Ac from early developmental stages onward can suppress disease development. Pregnant ht-mice were given Neu5Ac in their drinking water, and their mt-pups were given Neu5A-containing water according to the experimental schedule (Figure S2). At 2 months old, mt-mice and ht-mice, untreated or Neu5Ac-treated, were sacrificed for histological and urinary analysis.

The urinary albumin/creatinine ratio of the Neu5Ac-treated mt-mice was significantly reduced compared with untreated mt-mice, and was not significantly different from that of the Neu5Ac-treated ht-mice (Figure 7A). PAS-stained kidney sections of untreated and Neu5Ac-treated ht-mice appeared normal (Figure 7B left panel, and data not shown). Although the kidneys of untreated mt-mice were impaired, as described in Figure 3A (Figure 7B, middle panel), those of the Neu5Ac-treated mt-mice were much less affected. Enlarged glomeruli and dilatation of Bowman's spaces were rarely observed, and the mesangial matrix deposits were milder in the kidneys of the Neu5Ac-treated, compared with the untreated, mt-mice (Figure 7B right panel). Ultrastructural analysis showed that most of the podocyte foot processes in the Neu5Ac-treated mt-mice were well formed, and flattened and fused foot processes were observed less often than in untreated mt-mice (Figure 7C).

Since PC can be used as a marker for glomerular epithelial cells, we double-stained kidney sections with an anti-PC antibody and PNA to estimate the ratio of PNA-positive to total glomeruli (Figure 8). While PNA-positive glomeruli were not detected in ht

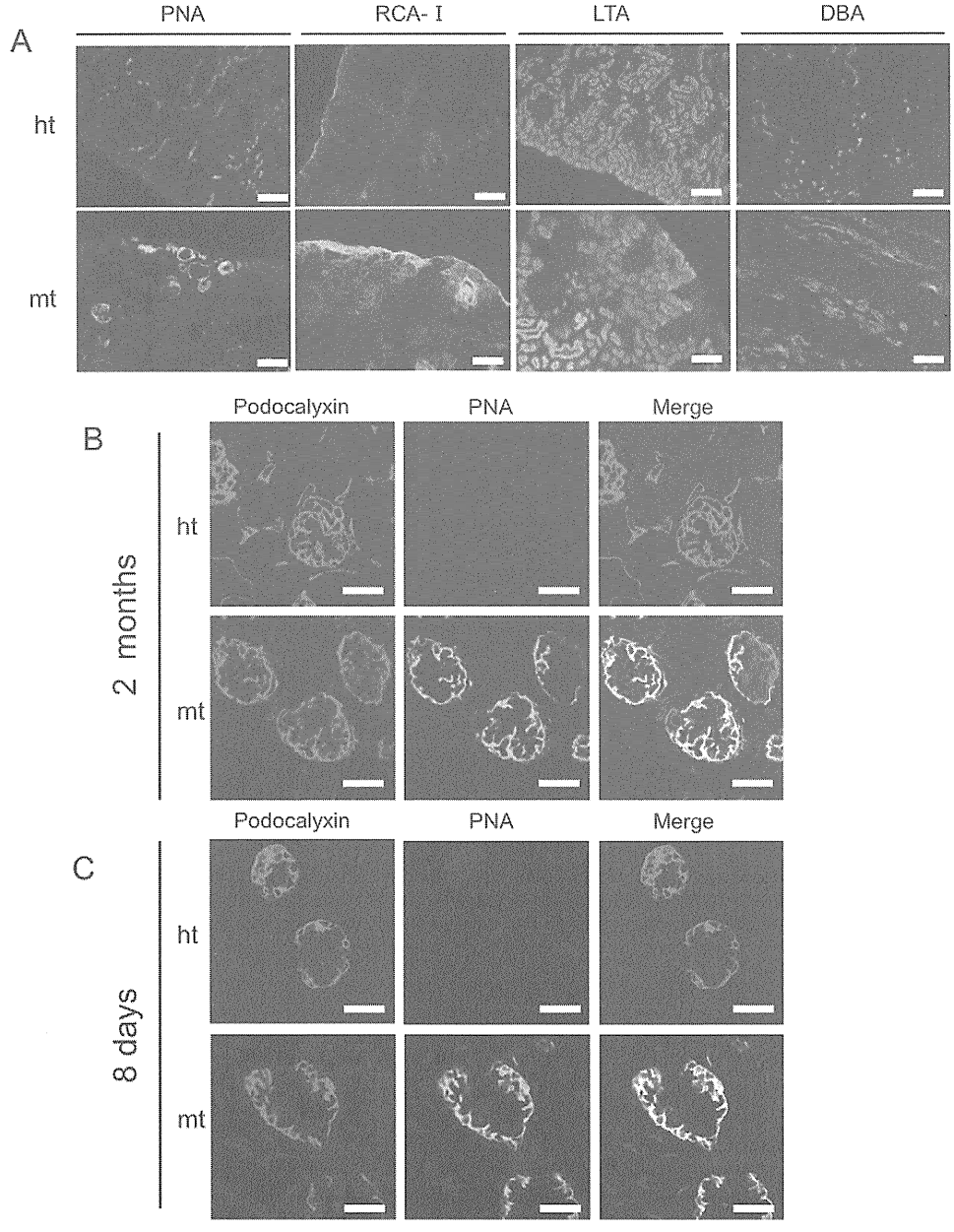

Figure 5. Lectin staining and glycan analysis of podocalyxin (PC) in kidneys. (A) Kidney sections stained with PNA, RCA-I, LTA, and DBA lectins (from left panels to right panels, respectively) in 3-month-old ht (upper panels) and mt (lower panels) mice. Scale bars: 120 μm. (B) Confocal laser scanning microscopic analysis of kidneys double-stained for PC and PNA, from 2-month-old ht (upper panels) and mt (lower panels) mice. Sections were stained with an anti-PC antibody (left panels; red), PNA (middle panels; green), and both (right panels; merge). Scale bars: 50 μm. (C) Confocal laser scanning microscopic analysis of kidneys double-stained for PC and PNA, from ht (upper panels) and mt (lower panels) mice at 8 days after birth. Sections were stained with the anti-PC antibody (left panels), PNA (middle panels; green), and both (right panels; merge). Scale bars: 50 μm.
doi:10.1371/journal.pone.0029873.g005

-mice, a large number of glomeruli were positive for PNA in the mt-mice (0% vs 56%) (Figure 8A, B). Neu5Ac treatment significantly reduced the proportion of PNA-positive glomeruli in the mt-mice (35%), indicating that Neu5Ac administration partially recovered the sialylation of PC and/or other glomerular glycoproteins and glycolipids.

Discussion

GNE is a dual-functioning enzyme, and various *GNE* gene point mutations have been identified in DMRV patients. To elucidate the pathological mechanisms of GNE point mutations and their effect on sialic acid biosynthesis, we generated mice with a GNE V572L point mutation found in Japanese DMRV patients [3]. We showed that the GNE V572L mt-mice had a shorter lifespan than wt- and ht-mice, and that they developed renal disorders with massive proteinuria shortly after birth. However, these mice did not exhibit apparent myopathies and motor dysfunction seen in DMRV (Figure S1B, S1C), and no renal disorder has been reported in DMRV patients. It is still not clear why the same V572L GNE point mutation caused different diseases in mice than those seen in humans. One possibility is that hyposialylation causes

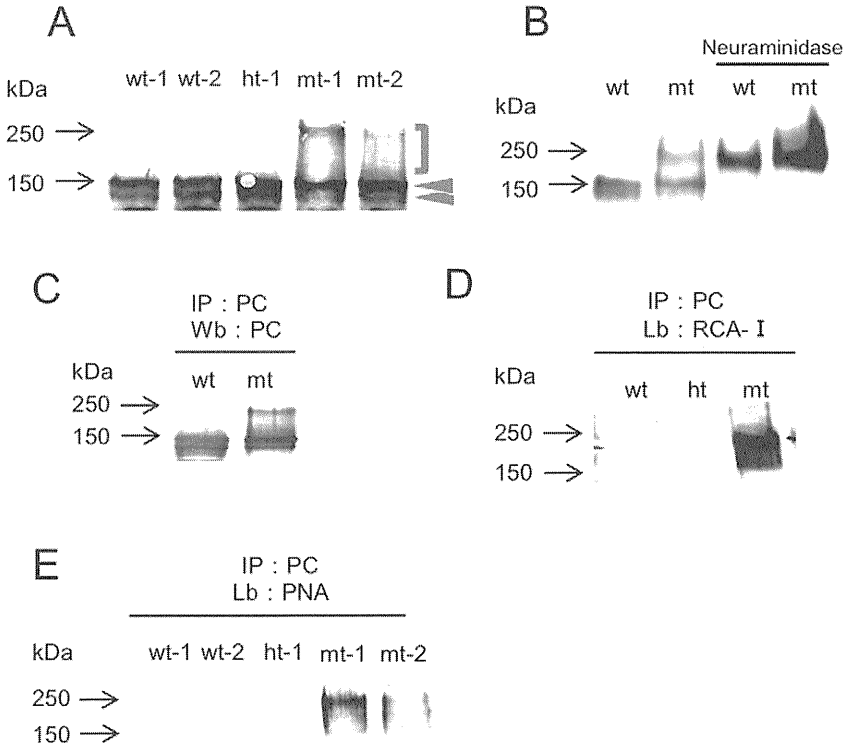

Figure 6. Western blot and lectin blot PC analysis. (A) Western blotting analysis of kidney lysates, using an anti-PC antibody. PC bands in wt and ht mice were about 140–150 kDa (arrowheads), while those in mt mice showed a shift to higher molecular weights (bracketed). (B) Neuraminidase treatment shifted the PC bands in wt mice to higher molecular weights similar to those seen in untreated mt mice. (C to E) Glycan analysis of PC by lectin blotting. After immunoprecipitation with an anti-PC antibody, PC bands were detected by PC (C), RCA-I (D), and PNA (E).
doi:10.1371/journal.pone.0029873.g006

the dysfunction of different tissues and cells in mice than in humans. To know such differences, it will be very informative to examine the sialylation status of glomeruli, especially the PC sialylation status, in human DMRV patients. Another possibility is that the molecular Neu5Ac and Neu5Gc sialic acid species might function differently in humans and mice, since humans, but not mice, are genetically defective in synthesizing Neu5Gc, a common mammalian sialic acid [34].

Furthermore, the phenotype of our mice was different than that of the two previously reported GNE point-mutant mice, a transgenic mouse carrying a human D176V point-mutant *GNE* gene in a mouse *GNE* gene-knockout background [20,21], and a knockin mouse carrying a GNE M712T point mutation [18]. The D176V GNE point-mutant mice exhibit myopathic features, but not renal disorders, while the M712 T point-mutant mice display severe renal hematuria and neonatal lethality, but not myopathy. The genetic situation of the D176V point-mutant mouse is different from the other two GNE mutant mice and from human DMRV patients, because the introduced human D176V point-mutant *GNE* gene is over-expressed. The M712T point-mutant mice suffer from far more severe renal disorders than those seen in our mice. It is not certain why the renal disorders differ between the two GNE-mutant mice. Although the V572L and M712T mutations are both located in the GNE kinase domain, they might affect different GNE functions. The V572L mutation may interfere with kinase domain dimerization, while the M712T mutation may change the GNE structure to affect in ATP catalysis, carbohydrate binding, and phosphoryl transfer [35]. These differences might affect the degree of hyposialylation of glycoproteins and glycolipids including PC.

Our mt-mice displayed glomerular defects with massive proteinuria shortly after birth, and had abnormally flattened and diffused podocyte foot processes. Their lifespan was significantly shortened by renal failure. These features resemble CNS, a very rare type of nephrotic syndrome. It is identified primarily in families of Finnish origin. Children born with the Finnish type of CNS die within a few months after birth due to massive proteinuria caused by impaired podocyte function [17,36,37]. The causative genes, *NPHS1*, which encodes nephrin and *CD2-accosiated protein*, which encodes CD2AP, have been identified in humans and mice [36,38–40]. These genes are expressed in glomerular epithelial cells in the kidney. Nephrin-deficient pups die with severe proteinuria immediately after birth. The kidneys of nephrin-deficient mice show fibrotic and hypercellular glomeruli, enlarged Bowman's spaces, dilated tubules, effaced podocyte foot processes, and the absence of slit-diaphragms, all characteristic features seen in human CNS. In heterozygous mice, approximately one third of the foot processes are fused, and nephrin mRNA levels are reduced [17,22,40]. On the other hand, CD2AP-deficient pups show proteinuria from two weeks of age onward, and most die of renal failure at six to seven weeks of age. They exhibit defective podocyte foot processes, accompanied by mesangial cell hyperplasia and extracellular matrix deposits similar to that found in nephrin-deficient mice. CD2AP associates with nephrin to form components of the slit diaphragms. Furthermore, heterozygous CD2AP mice also show proteinuria and glomerulosclerosis-like damage at nine months of age [17,22,38,39]. Therefore, the histological and pathological characteristics of our mt-mice resembled those of nephrin-deficient and CD2AP-deficient mice. However, our mt-mice survived longer than these

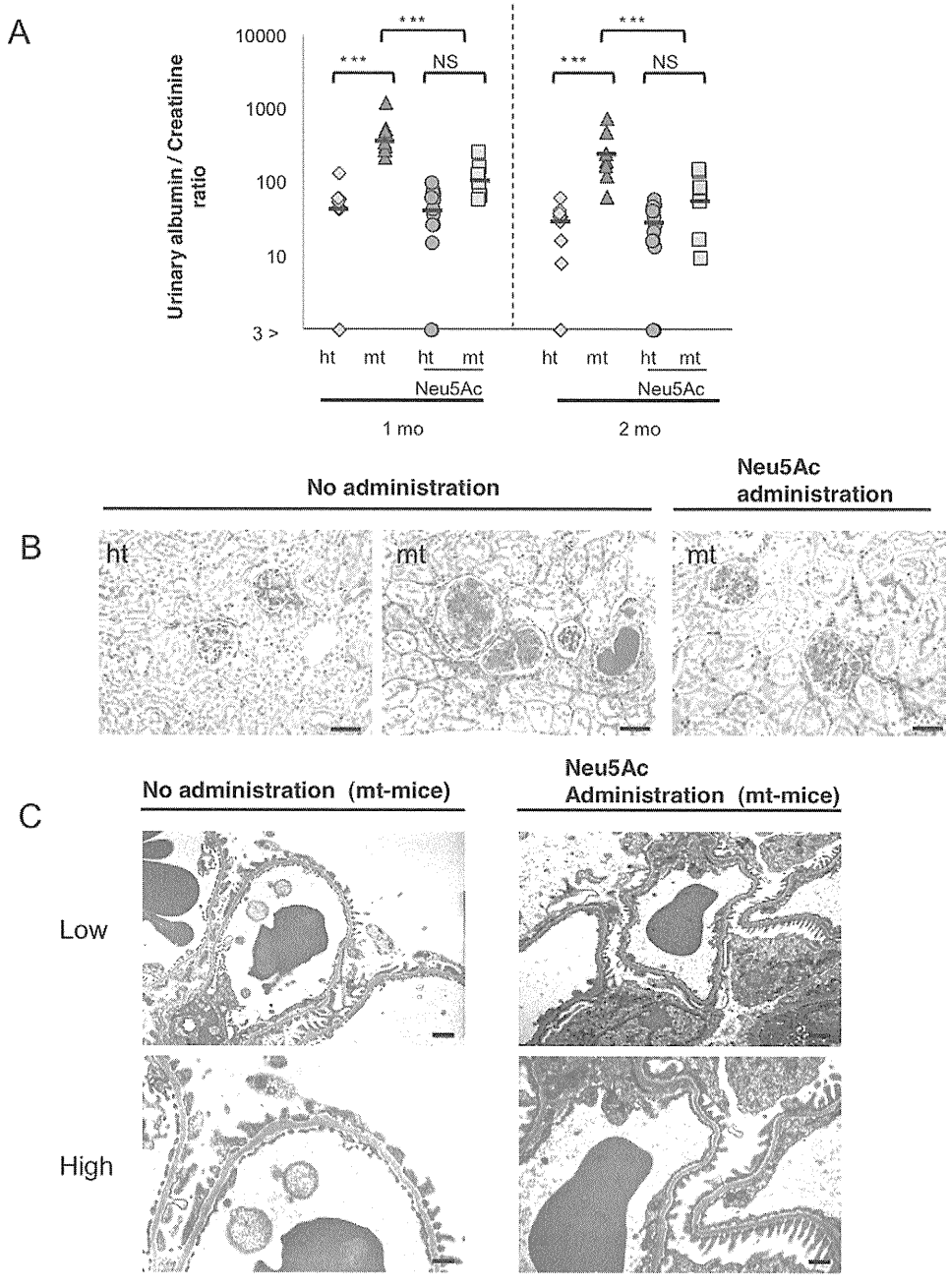

Figure 7. Urinary and histological analysis of mt mice treated with Neu5Ac. (A) Urinary albumin/creatinine ratios in untreated ht (green diamonds, n = 10) and mt (red triangles, n = 7) mice, and in Neu5Ac-treated ht (blue circles, n = 13) and mt (yellow squares, n = 8) mice at 1 and 2 months of age. ***$P<0.001$ (Two-way ANOVA). (B) PAS-stained kidney sections of untreated ht (left panel) and mt (middle panel) mice, and of Neu5Ac-treated mt (right panel) mice at 2 months old. Scale bars: 20 μm. (C) Electron microscopy of the glomeruli of mt mice at 2 months old that were untreated (left panels) or treated (right panels) with Neu5Ac. Low (upper panels, scale bars: 1 μm) and high magnification pictures (lower panels, scale bars: 500 nm).
doi:10.1371/journal.pone.0029873.g007

CNS model mice, and our ht-mice did not show adverse effects in the kidneys, suggesting that the GNE V572L point mutation had a milder effect on renal pathologies than that seen in the CNS model mice.

The formation of the nephrogenic zone and the number of nephrons in the renal cortex were comparable between neonatal mt-mice and ht-mice, suggesting that nephron development was not impaired and that nephronophthisis did not occur (Figure 4). On the other hand, by two months of age, the mt-mice had significantly fewer nephrons than did ht-mice, suggesting that nephron maintenance in these mice was affected by the glomerular damage with massive albuminuria. The remarkably enlarged glomeruli in the mt-mice might be caused by compensatory effects of the reduced number of nephrons.

The PNA and RCA-I lectin-staining patterns in the kidneys of the mt-mice were considerably different from those in the ht-mice (Figure 5); PNA-positive signals were detected in the glomeruli, and the RCA-I signals were more intense in the mt-mouse kidneys.

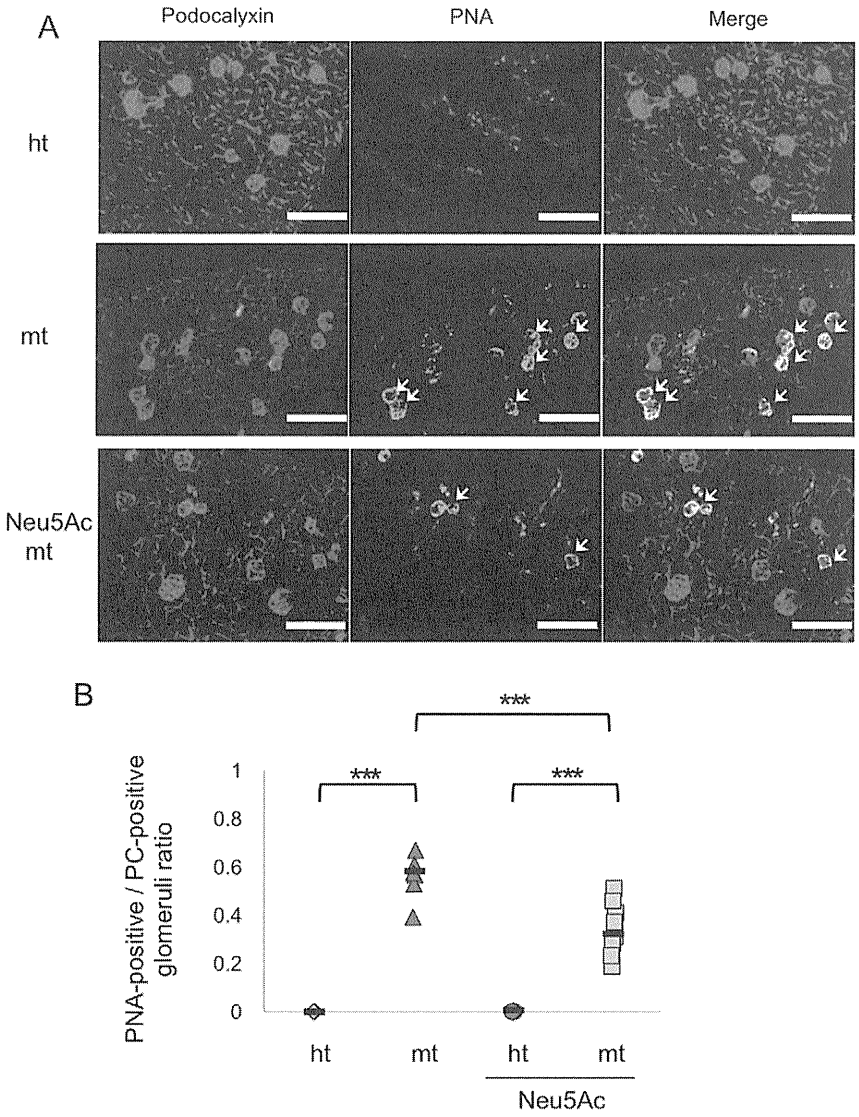

Figure 8. Reduced PNA-positive glomeruli ratios in Neu5Ac-treated mt mice. (A) Kidneys double-stained for PC and PNA, from untreated ht (upper panels) and mt (middle panels) mice, and Neu5Ac-treated mt mice (bottom panels). Sections were stained with an anti-PC antibody (left panels; red), PNA (middle panels; green), and both (right panels; merge). Scale bars: 200 μm. (B) Ratio of PNA-positive to PC-positive glomeruli in the kidneys of 2-month-old untreated ht (green diamonds, n = 4) and mt (red triangles, n = 6) mice, and of Neu5Ac-treated ht (blue circles, n = 5) and mt (yellow squares, n = 8) mice. ***$P<0.001$ (Two-way ANOVA).
doi:10.1371/journal.pone.0029873.g008

PNA-positive glomeruli are also observed in human glomerular disease, due to increased endogenous glomerular sialidase, and in diabetic nephropathy due to disturbed glycan turnover [41,42]. Since galactose-containing epitopes, Galβ1-3GalNAc and Galβ1-4GlcAc, which are recognized by PNA and RCA-I, respectively, are usually highly sialylated, these lectins cannot recognize these sialylated epitopes in ht-mice. Therefore, our results suggest that the GNE V572L mutation causes glycoproteins and glycolipids in the glomeruli to be highly hyposialylated. In western blot analyses of various glomerular epithelial proteins, only PC showed a mobility shift in the mt-mice. Neuraminidase treatment, immunoprecipitation/lectin blotting, and the colocalization of PC and PNA in the glomeruli confirmed that PC was highly hyposialylated in the mt-mouse kidney. PC hyposialylation is also observed in M712T mutant mice [18], suggesting that certain *GNE* point mutations cause PC hyposialylation. Since PC is a highly sialylated glycoprotein, its hyposialylation is easily detected by a mobility shift. We cannot rule out, however, the possibility that the sialylation of other glomerular epithelial proteins was slightly affected by the GNE mutation.

PC is a CD34-related sialomucin that is strongly expressed in podocytes. The negative charge of its highly sialylated extracellular domain makes PC important for maintaining the characteristic architecture of foot processes and the patency of slit-diaphragms [13,14,43–45]. PC-null mice die of anuric renal failure within twenty-four hours of birth [46]. They fail to form foot processes and slit-diaphragms, which impairs urine production. Interestingly, *CD34* and *endoglycan* mRNA expression in the kidneys was about two-fold higher in the mt-mice than in ht-mice, while the *PC* mRNA levels were comparable between the two (Figure S6). *CD34* mRNA levels are also increased in the kidneys of *PC*-null mice compared to wt-mice [46]. These results suggest that PC protein